Nano Research Energy

ISSN 2791-0091 (print); 2790-8119 (online)
https://doi.org/10.26599/NRE.2023.9120052

Review Article

Application of metal-organic frameworks, covalent organic frameworks and their derivates for the metal-air batteries

Yunyun Xu[1], Hairong Xue[1] (✉), Xijuan Li[1], Xiaoli Fan[2], Peng Li[1], Tengfei Zhang[1], Kun Chang[1], Tao Wang[1] (✉), and Jianping He[1] (✉)

[1] *Centre for Hydrogenergy, College of Materials Science and Technology, Nanjing University of Aeronautics and Astronautics, Nanjing 210016, China*

[2] *School of Materials Science and Engineering, Nanjing Institute of Technology, Nanjing 211167, China*

Received: 30 December 2022 / **Revised:** 23 January 2023 / **Accepted:** 25 January 2023

ABSTRACT

Metal-organic frameworks (MOFs) and covalent organic frameworks (COFs) as the novel porous materials have the merits of diverse, adjustable functionality, high porosity and surface area, which have great application prospects in the gas storage, separation and catalysis. In addition, their derivates make up for the insufficient of electronic conductivity and chemical stability of MOFs and COFs, and provide a new ideal for accurate control of material structure. Up to now, many efficient electrocatalysts have been designed based on MOFs, COFs and their derivates for O_2 reduction/evolution reactions (ORR/OER) and CO_2 reduction/evolution reactions (CO_2RR/CO_2ER) in the metal-air batteries. In this review, the latest development of MOFs, COFs and their derivates in the metal-air batteries is summarized, and we discuss the structural characteristics of these materials and their corresponding mechanisms of action. By comprehensively reviewing the advantages, challenges and prospects of MOFs and COFs, we hope that the organic framework materials will shed more profound insights into the development of electrocatalysis and energy storage in the future.

KEYWORDS

metal-organic frameworks, covalent organic frameworks, the derivates, electrocatalysis, metal-air batteries

1 Introduction

Global energy consumption has increased significantly, leading to an energy crisis and a serious greenhouse effect [1]. The development for clean and renewable energy is the basic requirement for sustainable development. In particular, the application of electrochemical energy storage and conversion not only reduces the consumption of traditional fossil fuels, but also brings new opportunities for the development of electrical installation [2].

In order to address above challenges, the metal-air batteries become the most promising candidate for energy storage and conversion because of their high specific energy, moderate price, high safety and environment-friendly (Fig. 1) [3–5]. Initially, the metal-oxygen batteries as the typical metal-air batteries are developed more earlier than metal-carbon dioxide batteries. The metal-oxygen (M-O_2) batteries consist of the metal anode (Li, Zn, Na, Al etc.), oxygen cathode, separator and electrolyte. The charge/discharge processes of the M-O_2 batteries include O_2 reduction and evolution reactions (ORR and OER), respectively. Additionally, the metal-carbon dioxide (M-CO_2) batteries with CO_2 as cathode active material include CO_2 reduction and evolution reactions (CO_2RR and CO_2ER) during discharge and recharge processes. More importantly, the M-CO_2 batteries are the new method for CO_2 fixation and energy storage, which can effectively decrease the emissions of CO_2 and provide a power source for the electrical device [4]. At present, the metal-air batteries involve a complex catalytic process of gas-liquid-solid phases, which make it difficult to deeply understand the mechanism of discharge and recharge processes. Moreover, aiming at the slow reaction kinetics of ORR, OER, CO_2RR and CO_2ER, it is necessary to develop an efficient bi-functional catalyst for the cathode to reduce the polarization and improve the cycle life of the batteries [6, 7].

Both as a kind of porous crystal materials, Metal-organic frameworks (MOFs) and covalent organic frameworks (COFs) have large surface area, high porosity and adjustable structure (Fig. 2) [10, 23–27]. Commonly, MOFs are synthesized by the self-assembly of metal-containing units and organic ligands, which has the open crystalline frameworks and permanent porosity [28]. The physical and chemical properties of primary building units further determine the functionality of MOFs. The abundant pores in the interior of MOFs enable fast mass transport of the target molecules to the inner surface, which is

Address correspondence to Hairong Xue, xuehr@nuaa.edu.cn; Tao Wang, wangtao0729@nuaa.edu.cn; Jianping He, jianph@nuaa.edu.cn

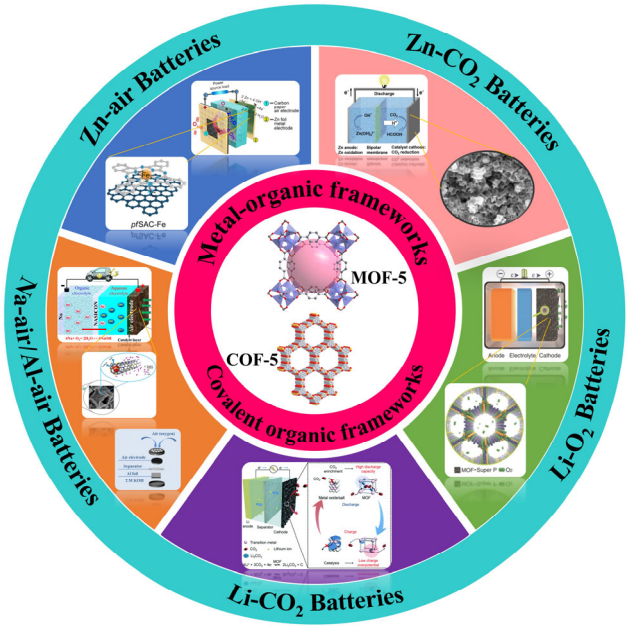

Figure 1 Summary of the metal-air batteries with MOFs and COFs as catalysts.

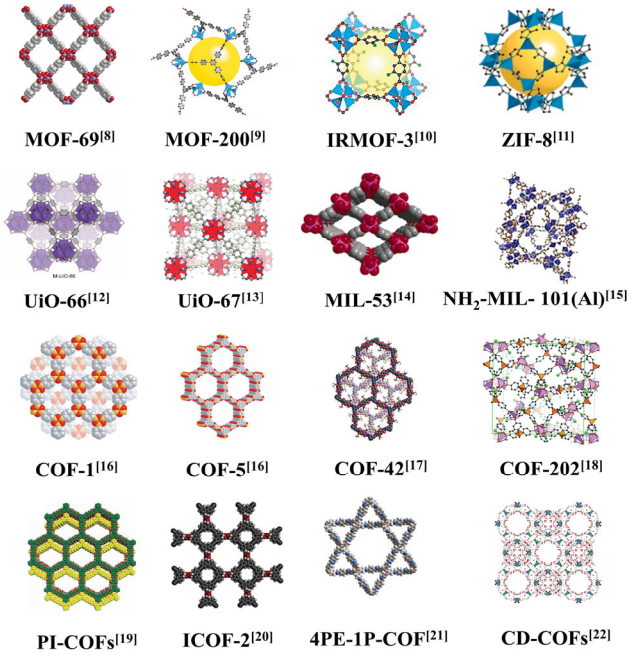

Figure 2 The typical structural of MOFs and COFs [8–22].

conducive to the catalytic activity of the reactions [29]. Furthermore, MOFs with high porosity also make the internal surface area relatively large, thus accelerating the reaction rate and extending the reaction range. Although high porosity is one of the fascinating features of MOFs, it needs to be combined with other features in order to turn MOFs into effective functional materials. By connecting longer organic ligand molecules with metal-containing units, we obtain the MOFs with larger pore size and rich porosity, which can provide more storage space and more adsorption sites. Large pore size is conducive to surface modification of various functional pores without sacrificing porosity. Although the use of MOFs in Li-ion batteries has been extensively studied [30–32], the unique gas adsorption/separation capability of MOF, making them has great potential valuable in metal-air batteries. Huang *et al.* designed and prepared Ru@Cu-HHTP as photocatalytic boosts CO_2 reduction to CO [33], in which they use the anionic metal-organic skeleton Cu-HHTP (HHTP=2,3,6,7,10,11-hexhydroxybenzoyl) as the host and the cationic photosensitizer $[Ru(phen)_3]^{2+}$(phen=1,10-phenanthroline) as the guest. Meanwhile, we should pay attention to the further separation of coordination groups may reduce the overall catalytic effect [34]. These MOFs with unsaturated metal sites can significantly produce high selectivity and molecular storage ability [26, 35, 36]. In 2005, Yaghi' group proposed the feasibility of CO_2 storage in MOFs materials at room temperature [10]. CO_2 is more likely to be absorbed on nitrogen by hydrogen bond or through interacting with the one pair of electrons. Therefore, MOFs are able to meet these requirements and widely used in the metal-air batteries, benefiting from their excellent gas adsorption and storage functions [37]. The following types of MOFs have been widely studied in recent years: isoreticular MOFs (IRMOFs) [28, 38], zeololite-imidazolate frameworks (ZIFs) [39, 40], materials of Institute Lavoisier (MILs) [41], university of oslo (UiO) [13]. Notably, MOF is used as a sacrificial template to derive a variety of porous materials that usually have high electrical conductivity and electrochemical reactivity. Furthermore, the design of single-atom catalysts (SACs) with high-efficiency catalytic activity through the MOFs derivates have been widely used in the field of electrocatalysis [42–44].

COFs are connected by strong covalent bonding with light elements (N, Si, B, C, and O), which are connected by the B-O, C-N, B-N, and B-O-Si linkages using the principles of reticular chemistry [18, 45, 46]. In 2005, Yaghi' group also firstly prepared the porous covalent organic skeleton through molecular building blocks, which was made up of six-membered ring and boroxine with permanent porosity [16]. This one-stop condensation reactions prove that the possibility of the synthesis of ordered COFs materials and achieves the desired structure by selecting different organic building units and regulating reaction conditions. In particular, we can carefully select building units and their assembly conditions to achieve pre-designed structure and performance [47]. COFs are firstly prepared by the self-condensation of boric acid to boroxine anhydride-based linkages (B_3O_3 rings). Additionally, boric acid can also react with catechols to boronate esters (COF-5) [16] and with silanols to borosilicate bonds (COF-202) [18] in the form of B-O and B-O-Si bonds, respectively [48]. COFs can also be designed by the formation of C-N bonds, including imine condensation (COF-300) [23], hydrazone linkages (COF-42) [17, 49], and azine linkages [50]. The synthesis of borazine ring linkages is also an existing form of B-N bonds in COFs [51]. COFs are characterized by unique advantages of controllable pore structures, low densities, large specific surface area, abundant metallophilic functional groups, high crystallinity and chemical robustness [19, 49, 52, 53]. The COFs with metal sites can improve the strength of the interaction between adsorbent and gas molecules, thus improving the capture and storage capacity. COFs with porous properties as the heterogeneous catalysts is very favorable because they not only have intrinsic activity but also can further combine with more active sites [54]. Likewise, COFs and their derivates have a wide range of applications in gas adsorption, photocatalysis, and energy storage [55, 56].

In this review, the development and recent progress of MOFs, COFs and their derivates in the metal-air batteries are

summarized (Fig. 3). The summary of recent progress in the metal-air batteries with MOFs, COFs and their derivates as catalysts is shown in Table 1. The MOFs and COFs with structural diversity and unique electrical properties has great potential for ORR, OER, CO_2RR and CO_2ER processes. Lastly, we propose insight views about the key challenges and

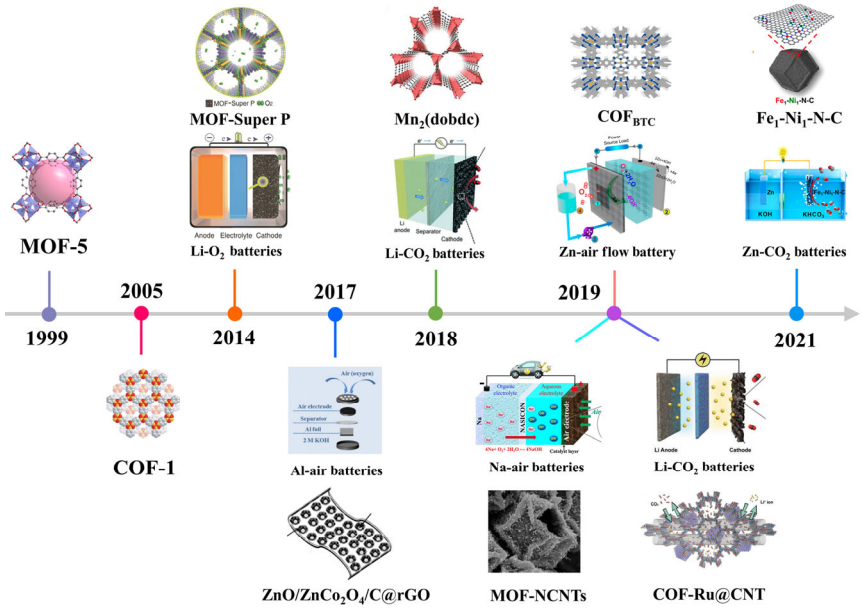

Figure 3 Timeline of the first application of MOFs and COFs in the metal-air batteries.

Table 1 Summary of recent progress in the metal-air batteries with MOFs, COFs and their derivates as catalysts

Metal-air batteries	Materials	MOF/COF	Function	Year	Ref.
Zn-air	Co porphyrin@ZIF-67	ZIF-67	ORR	2021	[67]
Zn-air	Ni-MOF/LDH	Ni-MOF	OER	2021	[68]
Zn-air	Mo-N/C@MoS_2	ZIF-8	ORR/OER	2017	[71]
Zn-air	Ni@N-HCGHF	Ni-BTC	ORR/OER	2020	[72]
Zn-air	Co-SAs@NC	ZnCo-ZIFs	ORR/OER	2019	[74]
Zn-air	CoNP-PTCOF	PTCOF	ORR/OER	2021	[77]
Zn-air	H-NSC@Co/NSC	COF@ZIF-67	ORR/OER	2022	[78]
Zn-air	pfSAC-Fe	COF	ORR	2019	[79]
Zn-air	mC-TpBpy-Fe	COF	ORR	2019	[80]
Zn-air	COF_{BTC}	COF	ORR	2019	[81]
Zn-CO_2	In/ZnO@C	ZIF-8	CO_2RR	2021	[83]
Zn-CO_2	Cu_3P/C	HKUST-1	CO_2RR	2019	[85]
Zn-CO_2	ZnTe/ZnO@C	ZnTe-MOF	CO_2RR/CO_2ER	2022	[86]
Zn-CO_2	Fe_1-Ni_1-N-C	ZIF-8	CO_2RR	2021	[88]
Li-O_2	Mn-MOF-74-Super P	Mn-MOF-74	ORR	2014	[96]
Li-O_2	Cu-THQ	c-MOF	ORR/OER	2021	[101]
Li-O_2	H-ZIF-8[5S]	ZIF-8	ORR/OER	2020	[102]
Li-O_2	Ru SAs-NC	ZIF-8	ORR/OER	2020	[103]
Li-O_2	UiO-67-Li/rGO aerogel	UiO-67	ORR/OER	2022	[104]
Li-CO_2	Mn_2(dobdc)	MOF	CO_2RR/CO_2ER	2018	[114]
Li-CO_2	MnTPzP-Mn	MOF	CO_2RR/CO_2ER	2021	[115]
Li-CO_2	Cu-TCPP	MOF	CO_2RR/CO_2ER	2022	[116]
Li-CO_2	Graphene@COF	COF	CO_2RR/CO_2ER	2019	[118]
Li-CO_2	COF-Ru@CNT	COF	CO_2RR/CO_2ER	2019	[119]
Li-CO_2	TTCOF-Mn	TTCOF-Mn	CO_2RR/CO_2ER	2021	[121]
Na-air	MOF-NCNTs	ZIF-67	ORR/OER	2019	[131]
Na-air	Co-N-C	ZnCo-MOF	ORR/OER	2020	[134]
Al-air	CuNC/KB-X	Cu-MOF	ORR	2018	[139]
Al-air	ZnO/$ZnCo_2O_4$/C@rGO	ZIF-67	ORR	2017	[140]

opportunities for MOFs and COFs in the electrochemical energy storage and conversion.

2 Metal-air batteries

MOFs and COFs as the catalysts of the cathode for the metal-air batteries should contains the following characteristics: (i) a fully reversible periodic structure for O_2/CO_2 absorption and emission; (ii) the exceptionally large pore apertures enable fast mass transport of the target molecules; (iii) the high thermal and chemical stability during reaction; (iv) the flexibility to achieve chemical functionalization and molecular fine-tuning to optimize absorption capacity. We have summarized the recent progress in the metal-air batteries with MOFs, COFs and their derivates as catalysts in Tables 2 and 3.

2.1 Zinc-air batteries

The zinc-air (Zn-air) batteries have advantages of high theoretical specific energy (1,350 Wh·kg^{-1}), low cost and environmental friendliness, leading to the great potential in the field of electronic products and electric vehicles [57]. A typical Zn-air battery contains catalyst of ORR/OER as cathode, Zn metal as anode, a separator and an aqueous alkaline electrolyte [58]. The mechanism of the Zn-air batteries for discharging and recharging reactions in alkaline aqueous electrolytes is as follows [59]:

Cathode: $O_2 + 4e^- + 2H_2O \leftrightarrow 4OH^-$ $E^\theta = 0.4$ V vs. SHE

Anode: $Zn + 4OH^- \leftrightarrow Zn(OH)_4^{2-} + 2e^-$

$Zn(OH)_4^{2-} \leftrightarrow ZnO + 2OH^- + H_2O$

$Zn + 2OH^- \leftrightarrow ZnO + H_2O + 2e^-$ $E^\theta = -1.25$ V vs. SHE

Overall reaction: $Zn + O_2 \leftrightarrow 2ZnO$ $E_{eq} = 1.65$ V vs. SHE

Because of the slow reaction kinetics of ORR and OER processes in the Zn-air batteries, we need to design an efficient bifunctional catalyst to improve the reaction energy barrier. The precious metal Pt and RuO_2 as catalysts show the highest electrocatalytic activity and the best stability for ORR and OER, respectively [60, 61]. However, it is difficult to achieve

Table 2 Summary of recent progress in the Zn/Al-O_2/CO_2 batteries with MOFs, COFs and their derivates as catalysts

Metal-air batteries	Cathode	Specific capacity (current density)	Open circuit voltage (V)	Peak power density (current density)	Durability (current density)	Ref.
Zn-air	Co porphyrin@ZIF-67	702 mAh·g^{-1} (20 mA·cm^{-2})	1.40	220 mW·cm^{-2} (2 mA·cm^{-2})	110 h (2 mA·cm^{-2})	[67]
Zn-air	Ni-MOF/LDH	—	—	—	600 cycles (10 mA·cm^{-2})	[68]
Zn-air	Mo-N/C@MoS_2	—	1.46	196 mW·cm^{-2} (5 mA·cm^{-2})	48 h (25 mA·cm^{-2})	[71]
Zn-air	Ni@N-HCGHF	706 mAh·g^{-1} (199 mA·cm^{-2})	1.49	117 mW·cm^{-2} (199 mA·cm^{-2})	20 h (10 mA·cm^{-2})	[72]
Zn-air	Co-SAs@NC	897 mAh·g^{-1} (20 mA·cm^{-2})	1.4	—	700 min (2 mA·cm^{-2})	[74]
Zn-air	CoNP-PTCOF	797 mAh·g^{-1} (10 mA·cm^{-2})	—	53 mW·cm^{-2} (10 mA·cm^{-2})	120 h (10 mA·cm^{-2})	[77]
Zn-air	H-NSC@Co/NSC	828 mAh·g^{-1} (10 mA·cm^{-2})	1.5	204 mW·cm^{-2} (5 mA·cm^{-2})	—	[78]
Zn-air	pfSAC-Fe	732 mAh·g^{-1} (100 mA·cm^{-2})	1.41	126 mW·cm^{-2} (140 mA·cm^{-2})	300 h (5 mA·cm^{-2})	[79]
Zn-air	mC-TpBpy-Fe	534 mAh·g^{-1} (50 mA·cm^{-2})	1.5	81 mW·cm^{-2} (140 mA·cm^{-2})	70 h (20 mA·cm^{-2})	[80]
Zn-air	COF_{BTC}	—	—	—	>80 h (10 mA·cm^{-2})	[81]
Zn-CO_2	In/ZnO@C	824 mAh·g^{-1} (1 mA·cm^{-2})	1.35	1.32 mW·cm^{-2} (10 mA·cm^{-2})	51 h (1 mA·cm^{-2})	[83]
Zn-CO_2	Cu_3P/C	—	1.5	2.6 mW·cm^{-2} (10 mA·cm^{-2})	—	[85]
Zn-CO_2	ZnTe/ZnO@C	—	1.35	0.93 mW·cm^{-2} (3 mA·cm^{-2})	36 h (1 mA·cm^{-2})	[86]
Zn-CO_2	Fe_1-Ni_1-N-C	—	—	—	15 h (1.1 mA)	[88]
Al-air	CuNC/KB-X	—	1.53	—	—	[139]
Al-air	ZnO/$ZnCo_2O_4$/C@rGO	42.6 mAh·g^{-1} (1 mA·cm^{-2})	1.53	—	—	[140]

Table 3 Summary of recent progress in the Li/Na-O_2/CO_2 batteries with MOFs, COFs and their derivates as catalysts

Metal-air batteries	Cathode	Specific capacity (current density)	Polarization (V)	Cycle number (current density)	Ref.
Li-O_2	Mn-MOF-74-Super P	9,420 mAh·g^{-1} (50 mA·g^{-1})	—	6 (200 mA·g^{-1})	[96]
Li-O_2	Cu-THQ	—	1.09 (1 A·g^{-1})	300 (1 A·g^{-1})	[101]
Li-O_2	H-ZIF-8[5S]	—	0.54 (50 mA·g^{-1})	—	[102]
Li-O_2	Ru SAs-NC	13,424 mAh·g^{-1} (0.02 mA·cm^{-2})	0.55 (0.02 mA·cm^{-2})	60 (0.02 mA·cm^{-2})	[103]
Li-O_2	UiO-67-Li/rGO Aerogel	6,891 mAh·g^{-1} (100 mA·cm^{-2})	0.6 (100 mA·cm^{-2})	115 (100 mA·cm^{-2})	[104]
Li-CO_2	Mn_2(dobdc)	18,022 mAh·g^{-1} (50 mA·g^{-1})	1.36 (100 mA·g^{-1})	50 (200 mA·g^{-1})	[114]
Li-CO_2	MnTPzP-Mn	14,025 mAh·g^{-1} (100 mA·g^{-1})	1.05 (100 mA·g^{-1})	90 (200 mA·g^{-1})	[115]
Li-CO_2	Cu-TCPP	20,393 mAh·g^{-1} (200 mA·g^{-1})	1.8 (2,000 mA·g^{-1})	123 (500 mA·g^{-1})	[116]
Li-CO_2	Graphene@COF	27,833 mAh·g^{-1} (75 mA·g^{-1})	1.70 (500 mA·g^{-1})	56 (500 mA·g^{-1})	[118]
Li-CO_2	COF-Ru@CNT	27,348 mAh·g^{-1} (200 mA·g^{-1})	1.24 (200 mA·g^{-1})	150 (400 mA·g^{-1})	[119]
Li-CO_2	TTCOF-Mn	13,018 mAh·g^{-1} (100 mA·g^{-1})	1.07 (100 mA·g^{-1})	180 (300 mA·g^{-1})	[121]
Na-air	MOF-NCNTs	—	0.3 (0.1 mA·cm^{-2})	35 (0.1 mA·cm^{-2})	[131]
Na-air	Co-N-C	—	0.31 (0.1 mA·cm^{-2})	20 (0.1 mA·cm^{-2})	[134]

large-scale application of noble metal electrocatalysts, owing to their limited reserves, high cost, and instable structure. Therefore, an excellent bifunctional electrocatalyst with low price, stable structure and porous properties can effectively promote OER and ORR in the Zn-air batteries [62, 63].

MOFs/COFs and their derivatives for the Zn-air battery

MOFs with the merits of particular pore structure and the controllability of metal sites can be served as both oxygen absorber and efficient electrocatalyst in the Zn-air batteries [64−66]. One of the most appealing molecular electrocatalysts is the molecule@support hybrids. Liang *et al.* grafted Co porphyrins on the surface of MOFs through ligand exchange and used them as catalysts in the Zn-air batteries [67]. The different hybrids can be formed based on the composition of MOF, optimizing the process of electron and mass transfer processes in the reaction of electrocatalytic. In addition, the active MOF supports can be used to further improve the activity and selectivity of catalytic processes. The Co porphyrin@MOF hybrids showing the considerable selectivity for ORR with 4e. Furthermore, because of the large specific surface area and abundant active sites of the MOFs, Zhang *et al.* constructed Ni-MOF/LDH heterostructures with high surface area and abundant phase interface by *in-situ* transformation through the strategy of "MOF on MOF", which shows the excellent OER catalytic activity [68]. In addition, MOFs can also be used as a sacrificial template to be transformed into other conductive electrocatalysts by calcination. We can obtain highly graphitized and amorphous carbon frameworks by direct carbonization of MOFs. However, we have to face the problems are that the pore size affects the diffusion and mass transfer process, and high graphitization causes the collapse of the active site [69, 70]. Amiinu *et al.* designed a multifunctional electrocatalyst (Mo-N/C@MoS_2) that the MoS_2 was vertically wrapped in a nitrogen-doped carbon (N/C) material derived from MOF by Mo-N interface coupling interaction [71]. The excellent multifunctional electrocatalytic property can be attributed to the unique three-phase active sites, in which the bare active site at the edge of MoS_2 nanosheet, the interface coupling center of Mo-N and the N-induced active site of adjacent C atoms in the framework. In addition, the hierarchical porous structure based on MOF-derivatives is beneficial to diffusion and mass transfer. As used in the solid-state Zn-air batteries, the efficiency and open-circuit voltage of Mo-N/C@MoS_2 reached 63.9% at 5 mA·cm^{-2} and 1.34 V, respectively. Yan *et al.* prepared a flexible self-supporting composite film by pyrolysis of Ni-based MOF/GO composite (denoted as 3D-CNT/rGO) for the Zn-air batteries (Fig. 4(a)) [72]. On

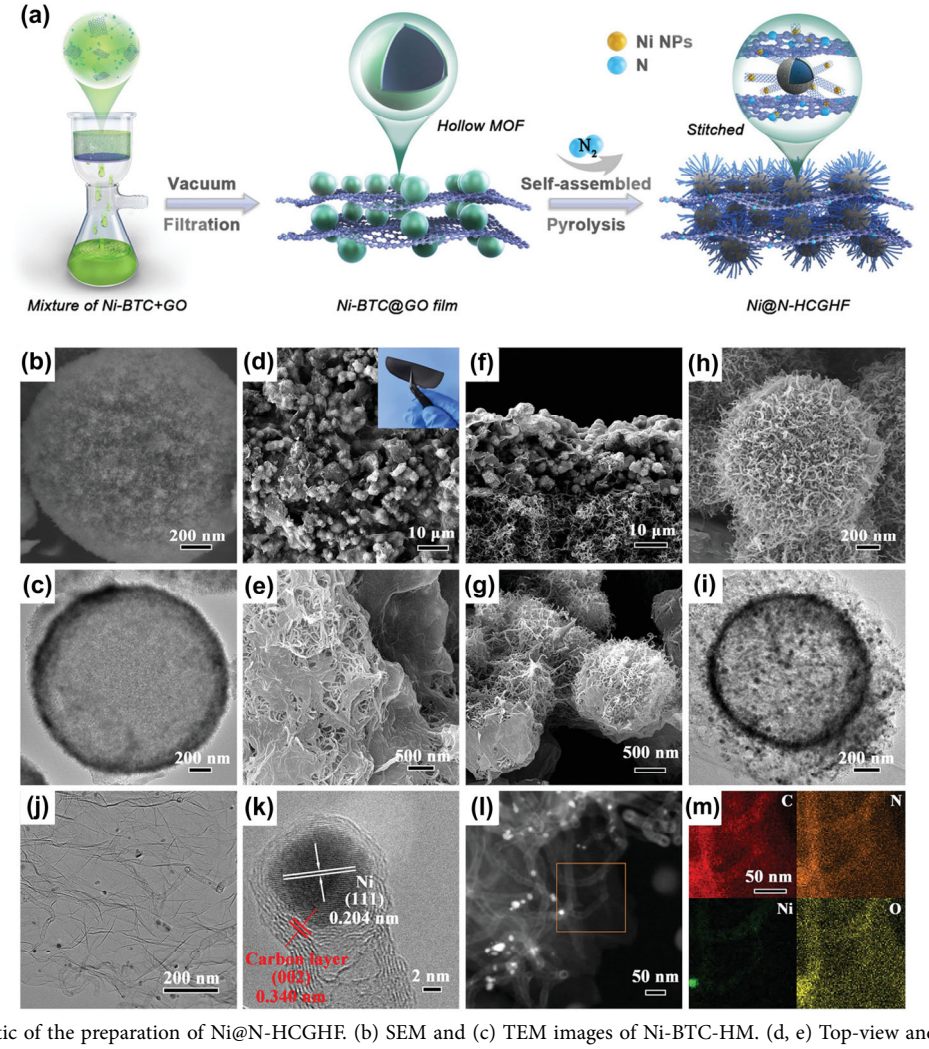

Figure 4 (a) Schematic of the preparation of Ni@N-HCGHF. (b) SEM and (c) TEM images of Ni-BTC-HM. (d, e) Top-view and (f, g) cross-sectional SEM images of Ni@N-HCGHF. (h) SEM and (i) TEM images of MOF-derived N-doped carbon nanotube hollow microsphere. (j) TEM, (k) HRTEM, (l) HAADF-STEM images, and (m) EDS mapping of Ni@N-HCGHF. Reproduced with permission from Ref. [72], © Wiley-VCH GmbH 2020.

the one hand, the superstructure of MOF-derived carbon nanotube microspheres can prevent the aggregation for rGO and provide a high specific surface area to generate more active sites (Figs. 4(b)–4(i)). On the other hand, carbon-based composite membrane has excellent electrical conductivity and can provide a channel for electron transfer (Figs. 4(j)–4(m)). Significantly, the efficient synergistic effect between the Ni core and carbon shell can reduce free energy and optimize the electrochemical reaction steps. MOFs have been recognized as the most potential candidates for the precise structural design of single-atom catalysts [73]. Han *et al.* successfully obtained the cobalt single atom on N-doped porous carbon (Co-SAs@NC) by precisely regulating the Zn-doping amount in bi-metallic ZnCo-ZIFs [74]. The single-atom Co catalyst shows excellent dual-function ORR/OER activity and durability in reversible Zn-air battery.

The strategy of accurately designing the active center of the bifunctional COFs electrocatalyst and adjusting its electronic structure is also one of the effective approaches to increase the activity of ORR and OER [75, 76]. Park *et al.* prepared pyridine-linked triazine COF-derivatives doped with Co nanoparticles (CoNP-PTCOF) [77]. The electronic structure of PTCOF was modulated by incorporation of Co nanoparticles to induce bifunctional activity for ORR and OER. The framework hybridization is a new development direction, and the main way is to connect MOFs and COFs through covalent bond to obtain hybrid materials. Li *et al.* produced core-shell carbon-based compounds (H-NSC@Co/NSC) by pyrolytically covalently linked COF@ZIF-67 as a bifunctional catalyst for ORR and OER (Fig. 5(a)) [78]. H-NSC@Co/NSC has a unique core-shell structure, which consists of a COF-derived hollow N, S co-doped carbon (H-NSC) core and a ZIF-67-derived carbon matrix (Co/NSC) shell inlaying with Co nanoparticles (NPs) (Figs. 5(b)–5(e)). On the one hand, the cavities in COF-derived have low density and high permeability, which is conducive to diffusion dynamics and makes the active site highly accessible to the surrounding reactants. On the other hand, the stable Co/NSC shell shows high activity for catalytic

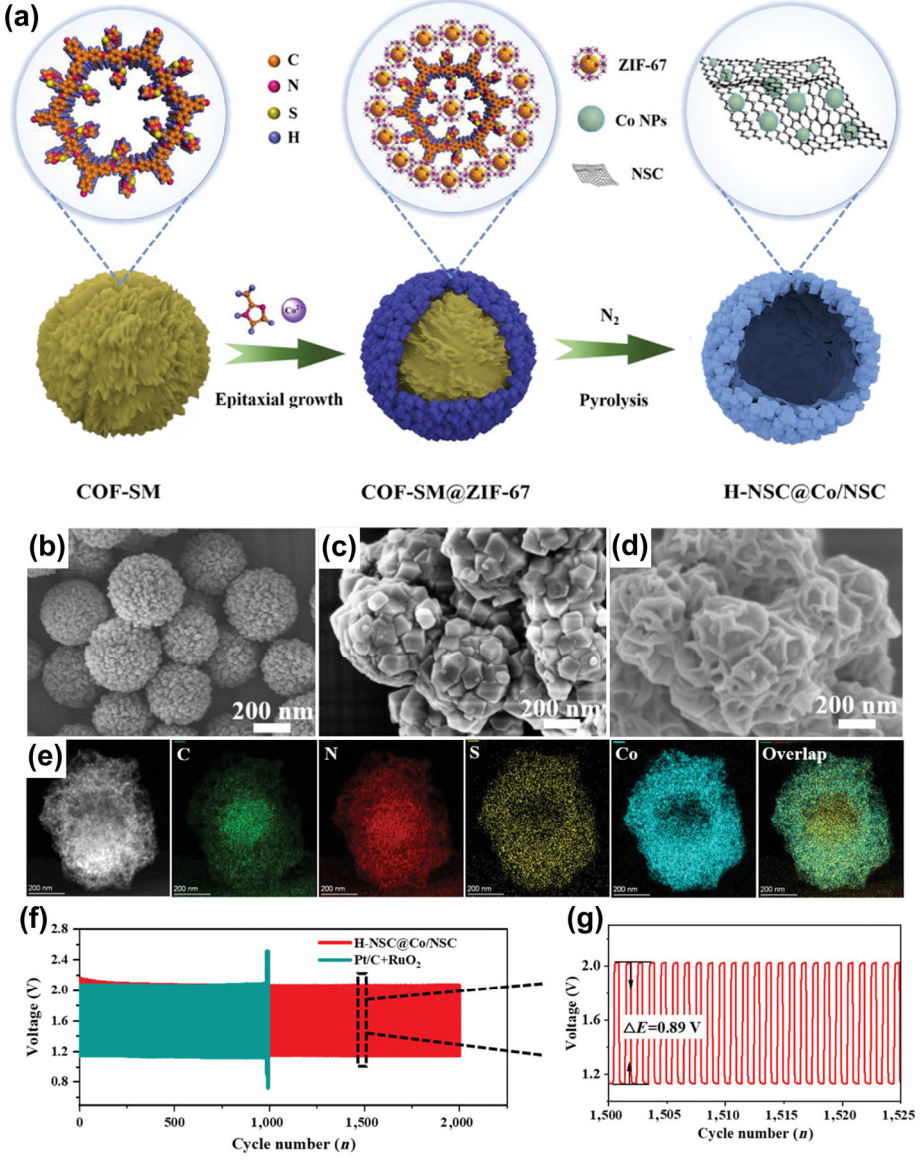

Figure 5 (a) The prepation of core-shell H-NSC@Co/NSC. SEM images of (b) COF-SM, (c) COF-SM@ZIF-67 and (d) H-NSC@Co/NSC. (e) HAADF-STEM and corresponding elemental mapping images of H-NSC@Co/NSC. (f, g) The discharge-charge curves of H-NSC@Co/NSC and Pt/C+RuO_2-based ZABs at 10 mA·cm^{-2}. Reproduced with permission from Ref. [78], © Wiley-VCH GmbH 2022.

OER/ORR. H-NSC@Co/NSC as bifunctional electrocatalyst for the Zn-air battery shows a power density of 204.3 mW·cm^{-2}, lower overpotential, and excellent cycle stability (Figs. 5(f) and 5(g)).

Peng *et al.* used a fully π-conjugated iron phthalocyanine (FePc) as COF to fabricate the well-defined Fe-N_4 single-atom catalysts (SACs) [79] (Figs. 6(a) and 6(c)). The pyrolysis-free synthesized SACs (pfSAC-Fe) is different from the random formation of Fe-N_4 moieties on a carbon matrix by pyrolysis (Figs. 6(b) and 6(d)). The π-electron conjugation structure between single-atom sites and graphene was constructed by using the intermolecular synergism between metal center and carbon matrix (Fig. 6(e)). In addition, the pfSAC-Fe has a stable cycle life of more than 300 h, and the performance is better than that of Pt/C (Fig. 6(f)). In general, the pfSAC-Fe as catalytic has good stability in Zn-air batteries and the pyrolytic-free synthesis strategy has potential applications in other electrochemical devices. Zhao *et al.* prepared a Fe-N doped mesoporous carbon (mC-TpBpy-Fe) as ORR catalyst for the Zn-air battery [80]. The mC-TpBpy-Fe was obtained through preparing a COF containing bipyridine by p-toluenesulfonic acid assisted mechanochemical method after carbonization and template removal. The bipyridine group in the COF is used to assist the coordination of Fe metal cites in mesoporous carbon materials. Moreover, the large pore size and abundant porosity of mesoporous carbon can effectively facilitate the diffusion of O_2 and electrolyte to the Fe-N_x active sites, which produces excellent ORR performance. Similarly, Peng *et al.* designed a functional COF (COF_{BTC}) as a catalyst of the cathode for the Zn-air flow batteries, which connected by a rigid conjugate skeleton and abundant Fe-N_4 active center [81]. The Fe single atom center can form strong interaction with hydroxide and other solvent molecules, resulting in *in-situ* intercalation and exfoliation of solvent molecules in solution. Importantly, the abundant nitrogen coordination Fe single atom structure (Fe-N-C) shows outstanding electrocatalytic activity for ORR. The results of the research provide a novel idea, method and reference for the development of soluble COFs in the Zn-air batteries.

The MOFs and COFs with high surface area, excellent thermal and chemical robustness are widely used in the Zn-air batteries. However, due to the low electrical conductivity of the most MOFs and COFs, the electrocatalysts need to be designed on the basis of their derivates. In fact, the intrinsic advantages of MOFs and COFs are not fully utilized. Achieving the high efficiency reactions of ORR and OER is also the first problem in the Zn-air batteries for us to solve it in the future by designing the appropriate MOFs and COFs-based catalysts.

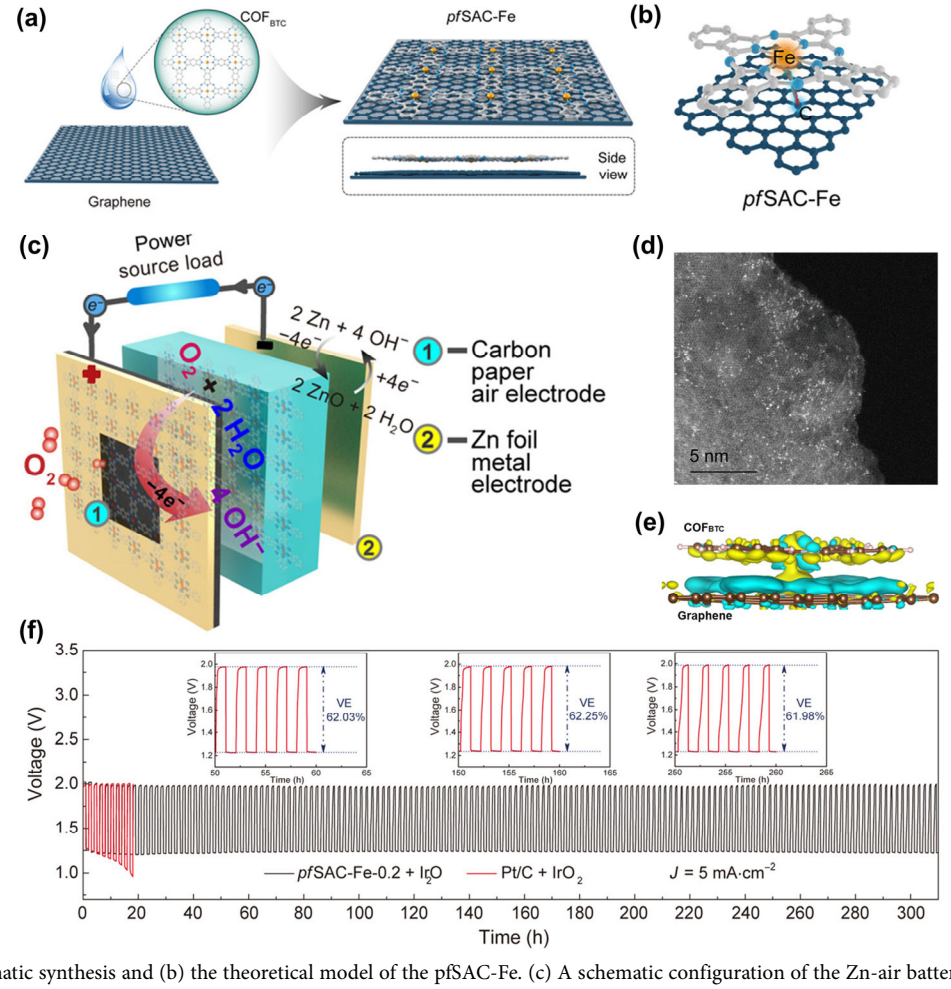

Figure 6 (a) Schematic synthesis and (b) the theoretical model of the pfSAC-Fe. (c) A schematic configuration of the Zn-air battery (d) HAADF-STEM of the pfSAC-Fe-0.2 (The bright dots are Fe atoms). (e) Differential charge density distribution on pfSAC-Fe. (f) The discharge-charge curves of the Zn-air batteries with Pt/C and pfSAC-Fe-0.2 as the ORR catalyst at 5 mA·cm^{-2}. Inset: voltage efficiency (VE) of the Zn-air batteries with pfSAC-Fe-0.2 as catalyst. Reproduced with permission from Ref. [79], © Peng, P. et al. some rights reserved; exclusive licensee American Association for the Advancement of Science 2019.

2.2 Zinc-carbon dioxide batteries

In the aqueous zinc-carbon dioxide (Zn-CO_2) batteries, the water acts as a proton-supplying medium to supply proton coupled electron transfer pathway and realize the electrochemical conversion of CO_2 to the value-added products (CO, HCOOH, C_2H_4, and C_2H_5OH) [82, 83]

$CO_2 + 2H^+ + 2e^- \rightarrow CO + H_2O$ $E^\theta = -0.11$ V
$CO_2 + 2H^+ + 2e^- \rightarrow HCOOH$ $E^\theta = -0.20$ V
$2CO_2 + 12e^- + 2H^+ \rightarrow C_2H_4 + 4H_2O$ $E^\theta = 0.07$ V
$2CO_2 + 12e^- + 2H^+ \rightarrow C_2H_5OH + 3H_2O$ $E^\theta = 0.08$ V

In addition, the CO_2RR process has a large Gibbs free energy without using catalyst, and the activation process involving an electron requires a large overpotential [82]. In addition to the activity of the catalysts, the competitive relationship between the CO_2RR and the HER needs to be further considered. To realize the reversible aqueous Zn-CO_2 batteries, it is necessary to design catalysts with efficient bifunctional for CO_2RR and CO_2ER processes. Xie *et al.* group have successfully prepared a three-dimensional (3D) porous Pd with rich edge by hydrogen evolution assisted electrodeposition, and realized a reversible conversion of CO_2 to liquid HCOOH in the aqueous Zn-CO_2 battery [84]. The discharging and recharging reactions are as follows:

Cathode: $CO_2+2H^++2e^- \leftrightarrow HCOOH$ $E_c = -0.294$ V
Anode: $Zn - 2e^- \leftrightarrow Zn^{2+}$
$Zn^{2+} + 4OH^- \leftrightarrow Zn(OH)_4^{2-}$
$Zn(OH)_4^{2-} \leftrightarrow ZnO + 2OH^- + H_2O$ $E_a = -1.249$ V
Overall reaction: $Zn + CO_2 + 2H^+ + 2OH^- \leftrightarrow$
$ZnO + HCOOH + H_2O$. $E_{theo} = E_c - E_a = 0.955$ V

The enriched electrochemical active surface of 3D porous Pd promotes the selective reduction of CO_2 to HCOOH, and as well as the selective oxidation of HCOOH to CO_2 at low overpotential [81]. More importantly, two bipolar membranes in opposite directions achieving a two-compartment discharging and charging processes. The reversible aqueous Zn-CO_2 batteries at current density of 0.56 mA·cm^{-2} with lower overpotential is 0.19 V, higher energy efficiency is 81.2%, and over 100 cycle life.

MOFs and their derivatives for Zn-CO_2 battery

MOFs have been widely used as sacrificial templates to prepare the functional porous materials for the catalysts of the Zn-CO_2 batteries. In 2019, Xu *et al.* reported a Cu_3P/C nanocomposite by phosphorylation of the Cu-based MOFs precursor as electrocatalyst for Zn-CO_2 batteries [85]. The good catalytic performance for CO_2RR due to the synergistic catalytic effect of Cu, P. In particular, the carbonization of MOFs facilitates the preparation of highly conductive and stable copper/porous carbon composites. Teng *et al.* designed a hollow nanocubic In/ZnO@C derived from an $In(OH)_3$-doped of Zn-MOF (Figs. 7(a)–7(d)) [83]. *In-situ* introduction of $In(OH)_3$ into Zn-MOF with unique nanocube morphology can effectively avoid the agglomeration of In metal (Figs. 7(e)–7(g)). The In/ZnO@C exhibites favourable catalytic activity and selectivity for CO_2 conversion to formate. Subsequently, Teng *et al.* prepared a heterostructured materials (ZnTe/ZnO@C) as a Zn-based electrocatalyst for the Zn-CO_2 batteries by using a novel ZnTe as MOFs supported on N-doped carbon nanosheets (Figs. 7(h) and 7(i)) [86]. Significantly, the formation of formate is achieved by stabilizing key HCOO* intermediates on ZnTe. Due to the flexibility and controllability of structure and composition regulation, MOFs is one of the ideal candidates for accurate building of adjacent single atom site in the Zn-CO_2 batteries [87].

MOFs have great advantageous in the accurate construction of single-atom catalysts (SACs) in the Zn-CO_2 batteries. Jiao *et al.* proposed a Zn-assisted atomization strategy (ZAAS), which introduced Fe and Ni single atoms into MOF-derived nitrogen-doped carbon, and successfully constructed Fe_1-Ni_1-N-C with adjacent non-bonded Fe-Ni atom pairs (Figs. 8(a)–8(c)) [88]. The Fe single atom in Fe_1-Ni_1-N-C catalyst can be activated by the adjacent Ni single atom through non-bonding interaction, which promotes the generation of COOH* intermediates to accelerate the reduction of CO_2 (Fig. 8(d)). Thus, the Fe_1-Ni_1-N-C shows excellent a FE_{CO} of 96.2% and operation durability (Figs. 8(e) and 8(f)).

The studies of MOF-based catalysts in the Zn-CO_2 batteries are still at an early stage. We believe that the precise construction of MOF-based catalysts with high crystallinity and chemical robustness will be beneficial in transforming CO_2 electrochemistry into low-cost, controllable value-added products and expand the performance at high current density in the future.

2.3 Lithium-oxygen batteries

Lithium-oxygen (Li-O_2) batteries with a theoretical energy density of 3,505 Wh·kg^{-1} (based on Li_2O_2) and operational voltage of 2.96 V, play an important role to realize the conversion of chemical energy to electric energy [89, 90]. A typical non-aqueous Li-O_2 batteries consist of dissolution/deposition process of lithium anode, the ORR/OER processes at the gas diffusion cathode, and the organic electrolyte with high conductivity of Li^+ [91].

The mechanism of charge and discharge reactions are as follows:

Anode: $2Li - 2e^- \rightarrow 2Li^+$
Cathode: $Li^+ + e^- + O_2 \rightarrow LiO_2$ $E^\theta = 3.0$ V (vs. Li/Li$^+$)
$LiO_2 + Li^+ + e^- \rightarrow Li_2O_2$ $E^\theta = 2.96$ V (vs. Li/Li$^+$)
Overall reaction: $Li + O_2 \leftrightarrow Li_2O_2$

During the discharging and charging processes, the ORR and OER processes take place on the cathode. The slow kinetic process of the cathode occurs at the three-phase interface (oxygen/electrode/electrolyte). The Li_2O_2 as an insulating product is deposited on the surface of catalysts during the discharge process, which further inhibits the transportation of oxygen and electron [92]. Therefore, it is essential to develop an efficient catalyst with high oxygen adsorption ability and bifunctional catalytic activity for ORR and OER.

Zhang *et al.* directly grew Mn-MOF-74 nanoparticles on carbon nanotubes (Mn-MOF-74@CNTs), which worked in humid oxygen environment and obtained LiOH as the discharge product [93]. It is further reported that LiOH is formed through the chemical conversion of Li_2O_2 in the metal center of Mn^{2+}/Mn^{3+}. The related reactions are as follows [93]:

$2Li^+ + 2O_2 + 2e^- \rightarrow 2LiO_2$(sol.)
$2LiO_2$(sol.) $\rightarrow Li_2O_2 + O_2$
$Li_2O_2 + 2H_2O \leftrightarrow 2LiOH + H_2O_2$
$H_2O_2 \rightarrow H_2O + \frac{1}{2}O_2$
Overall reaction: $2Li^+ + \frac{1}{2}O_2 + H_2O + 2e^- \rightarrow 2LiOH$

This moist oxygen environment and the design of MOF-based

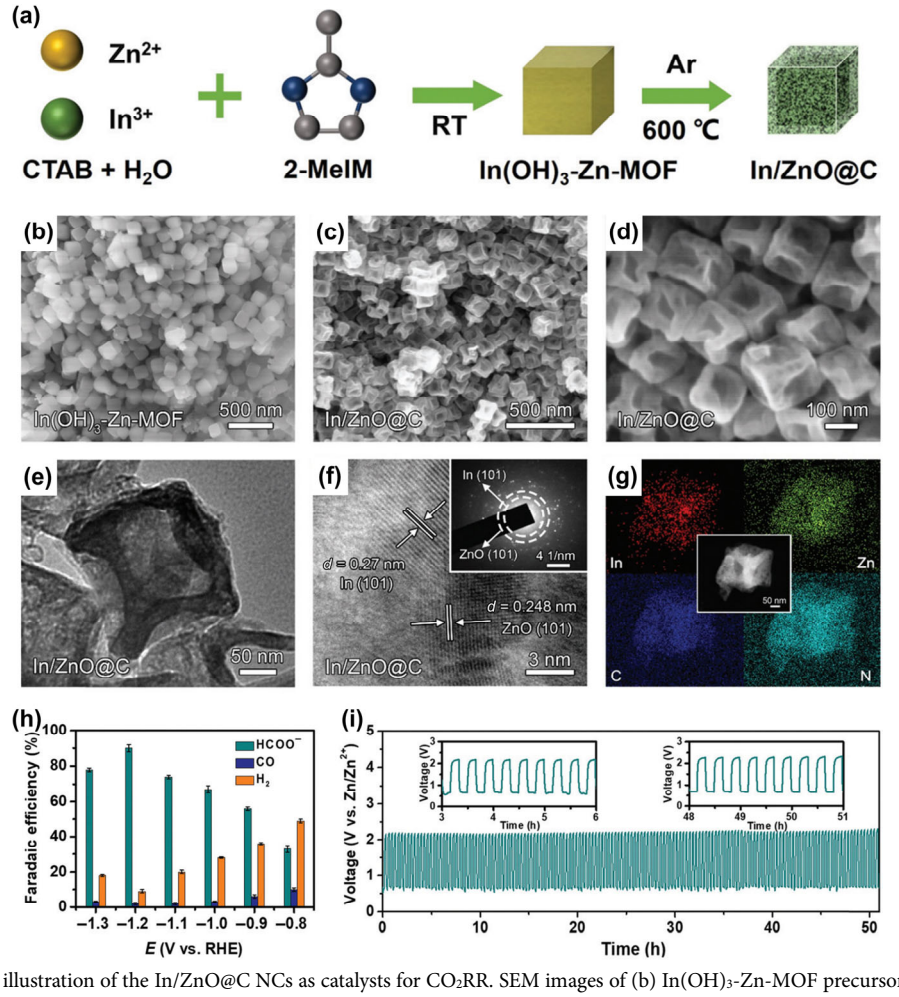

Figure 7 (a) Schematic illustration of the In/ZnO@C NCs as catalysts for CO_2RR. SEM images of (b) $In(OH)_3$-Zn-MOF precursors and (c, d) In/ZnO@C. (e) TEM, (f) HRTEM, and (g) elemental mapping images of In/ZnO@C. (h) Variation in FE_{HCOO^-}, FE_{CO} and FE_{H_2} for In/ZnO@C with the applied potential. (i) The discharge-charge curves at 1 mA·cm^{-2}. Reproduced with permission from Ref. [83], © The Royal Society of Chemistry and the Chinese Chemical Society 2021.

functional electrocatalyst contribute to the formation of main discharge product LiOH and the excellent cycle life of Li-O_2 batteries.

The practical application of Li-O_2 battery has been hindered by the high polarization on ORR and OER processes, the hole blockage of air cathode caused by discharge product (Li_2O_2), and electrolyte instability, leading to poor energy efficiency and cycle performance.

MOFs and their derivatives for Li-O_2 battery

MOFs has the merits of open metal sites, high surface area, uniform pores and adjustable chemical environment, which can significantly improve the adsorption ability for O_2 as well as facilitate Li^+ diffusion and products deposition [94]. In 2014, Li *et al.* firstly prepared a novel cobalt-containing MOFs as template for the transition metal-N-C as ORR catalyst in the non-aqueous Li-O_2 batteries [95]. *In-situ* preparation of N-doped graphene/graphene tube nanocomposites by using MOFs as a template provides a novel way to prepare carbon nanocomposites. Subsequently, Wu *et al.* firstly applied MOFs as O_2 electrode for Li-O_2 batteries (Fig. 9(a)) [96]. The discharge capacity of Mn-MOF-74 combined with Super P as cathode catalyst is 9,420 mAh·g^{-1}, which is more than four times bigger than that of the battery with only Super P (Fig. 9(b)). A series of MOFs for oxygen electrocatalysts have been developed [97–99]. Furthermore, the electronic insulation properties of traditional MOFs are due to the big energy barrier for electron transfer between the rigid metal ions and redox inactive organic ligands [100]. This problem can be improved by developing new conductive MOF materials or by combining them with good conductors. Majidi *et al.* reported a copper tetrahydroxyquinone (Cu-THQ) conductive MOF (c-MOF) as the catalyst of cathode for the Li-O_2 batteries without conductive additives [101]. Owing to the existence of c-MOF with high active surface area, the formation of electron-conductive nanocrystals Li_2O_2 in amorphous Li_2O_2 region can be promoted. Choi *et al.* developed multilayer MOFs with alternating stabilizing layers and decomposing layers to automatically produce and stabilize sub-nanoparticles (SNPs) in scalable batch loading (Figs. 10(a)–10(c)) [102]. Importantly, the stability of SNPs is achieved by π-antibonding through the multiple shell layer and the interlayer hopping mechanism can significantly minimizes the transmission resistance of hollow interspaces to obtain high conductivity (Figs. 10(d) and 10(e)).

Moreover, it's also a common way to obtain catalysts with high activity and stability by precise regulation at atomic scale with the MOFs assisted strategy in the Li-O_2 batteries. Hu *et al.* synthesized a binder-free, porous structure, stable and efficient bifunctional Ru single-atom electrocatalyst for ORR and OER processes (Fig. 11(a)) [103]. The Ru single atom on N-doped

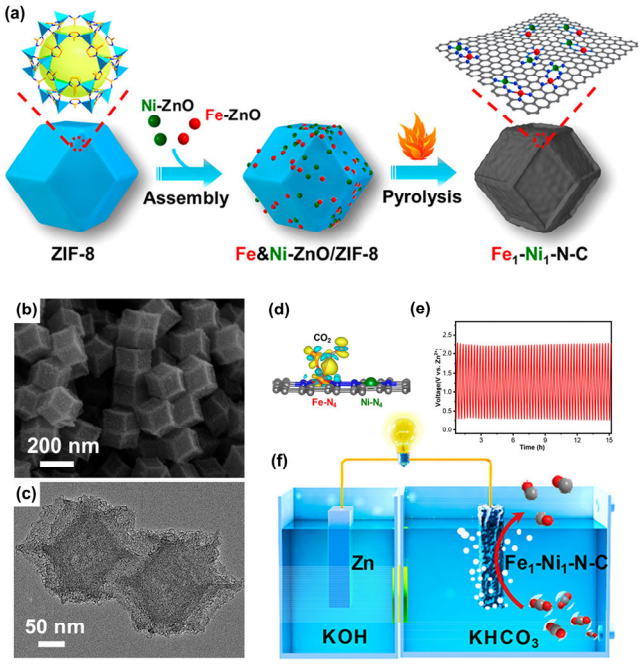

Figure 8 (a) Schematic construction of Fe_1-Ni_1-N-C. (b) SEM and (c) TEM images of Fe_1-Ni_1-N-C, (d) electron density difference analysis of CO_2 adsorbed on Fe-N_4 sites of Fe_1-Ni_1-N-C (yellow and cyan stands for charge accumulation and depletion). (e) The discharge-charge curves test at 1.1 mA. (f) Illustration for the aqueous rechargeable Zn-CO_2 battery using Fe_1-Ni_1-N-C at the cathode. Reproduced with permission from Ref. [88], © American Chemical Society 2021.

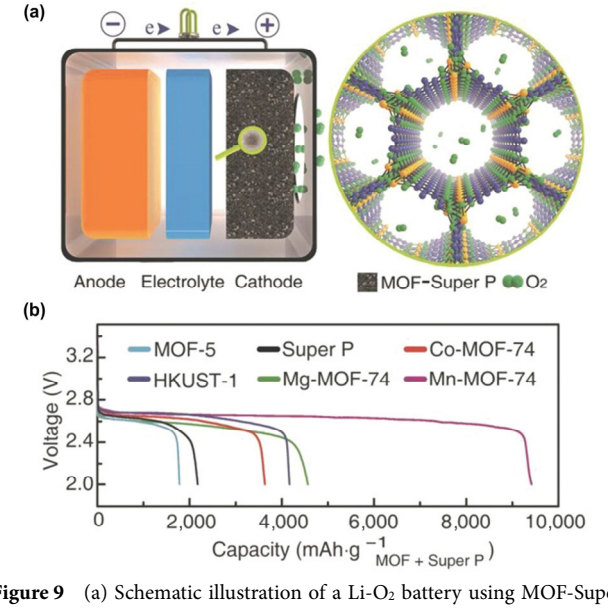

Figure 9 (a) Schematic illustration of a Li-O_2 battery using MOF-Super P composite as catalyst. (b) Discharge profiles of the Li-O_2 batteries under O_2 atmosphere with a current of 50 mA·g^{-1}. Reproduced with permission from Ref. [96], © WILEY-VCH Verlag GmbH & Co. KGaA, Weinheim 2014.

porous carbon (Ru SAs-NC) catalyst was prepared by the MOF-assisted space confinement and ionic replacement strategies, which can significantly reduce the overpotential of discharge and charge reactions and greatly improve the electrochemical performance of Li-O_2 batteries (Fig. 11(h)). In particular, the molecular cage of the metal-organic frameworks plays an essential role in space confinement (Figs. 11(b)–11(d)). The Zn site will volatilize during high-temperature pyrolysis process, and Ru^{3+} can replace the Zn^{2+} node to form the Ru-N coordination structure (Figs. 11(e)–11(g)).

Though the metal-air batteries are open system, the generation of dendrites and the effect of O_2 on the anode can be reduced by optimizing the diaphragm. Xu's group developed a new solid-state electrolyte material UiO-67-Li with molecular pore conduction of Li based on the MOF-derivates, thereby building an integrated solid-state Li-O_2 batteries with high stability and safety [104]. Furthermore, the solid electrolyte material UiO-67-Li was grown *in-situ* on porous conductive graphene aerogel (denote as UiO-67-Li@rGO aerogel). Then the cathode with good solid-solid contact interface were successfully constructed, which could realize the ion/electron transport and the rapid gas diffusion. The abundant unsaturated sites and oriented Li^+ transport channels in the UiO-67-Li skeleton will cause rapid dissociation of lithium salts. The dissociated anions will be fixed by the unsaturated sites exposed in the skeleton, resulting in an increase in the number of freely moving Li^+, thereby increasing the ionic conductivity and the number of Li^+ migration for electrolyte. The solid-state Li-O_2 battery with UiO-67-Li@rGO aerogel exhibits stability up to 115 cycles, low polarization of 0.8 V, and excellent performance. Zhou's group prepared a MOF-based separator for Li-O_2 batteries [105]. The MOFs-based membranes can isolate the liquid negative electrode and confine the redox medium to the positive electrolyte to avoid shuttle effect. Deng *et al.* investigated an organic oxygen battery with liquid lithium-based anode and MOF membranes (Fig. 12(a)). An organic liquid Li-based negative electrode was obtained by dissolving an equal molar ratio of lithium metal in 1, 2-dimethoxyethane biphenyl (Bp-Li). However, the MOFs-based membranes of zeolite imidazolium skeleton (ZIF-7) effectively prevent BP-Li transmission to the side of cathode (Figs. 12(b)–12(e)) [106]. Electrochemical performance of organic O_2 batteries based on BP-Li anode at different rates shows that the stable discharge plateau and charging plateau at ~2.45 and ~2.75 V at low current density, respectively. A high current density of 4,000 mA·g^{-1} and a high reversible specific capacity of 2,000 mAh·g^{-1} can be achieve with 100 cycles (Fig. 12(f)).

MOFs have adjustable pore channels and open metal sites that facilitate mass transfer, O_2 enrichment and ORR/OER catalytic processes. In addition, the periodic structure and chemical stability of MOFs-based catalysts are also ideal choices for the Li-O_2 batteries.

2.4 Lithium-carbon dioxide batteries

Among many metal-air batteries, Lithium-carbon dioxide (Li-CO_2) battery with high specific energy density (1,876 Wh·kg^{-1}) and discharge potential (2.84 V) has become a kind of new energy conversion and storage device for the next generation due to the especial active material CO_2 [4, 107, 108]. In 2011, Takechi *et al.* constructed a non-aqueous Li-O_2/CO_2 batteries with Ketjen-black as cathode catalyst, which obtained the capacity is three times than pure Li-O_2 batteries [109]. The reaction mechanism of Li-O_2/CO_2 batteries are proposed as follows:

$$4O_2 + 4e^- \rightarrow 4O_2^{\bullet-}$$
$$O_2^{\bullet-} + CO_2 \rightarrow CO_4^{\bullet-}$$
$$CO_4^{\bullet-} + CO_2 \rightarrow C_2O_6^{\bullet-}$$
$$C_2O_6^{\bullet-} + O_2^{\bullet-} \rightarrow C_2O_6^{2-} + O_2$$
$$C_2O_6^{2-} + 2O_2^{\bullet-} + 4Li^+ \rightarrow 2Li_2CO_3 + 2O_2$$

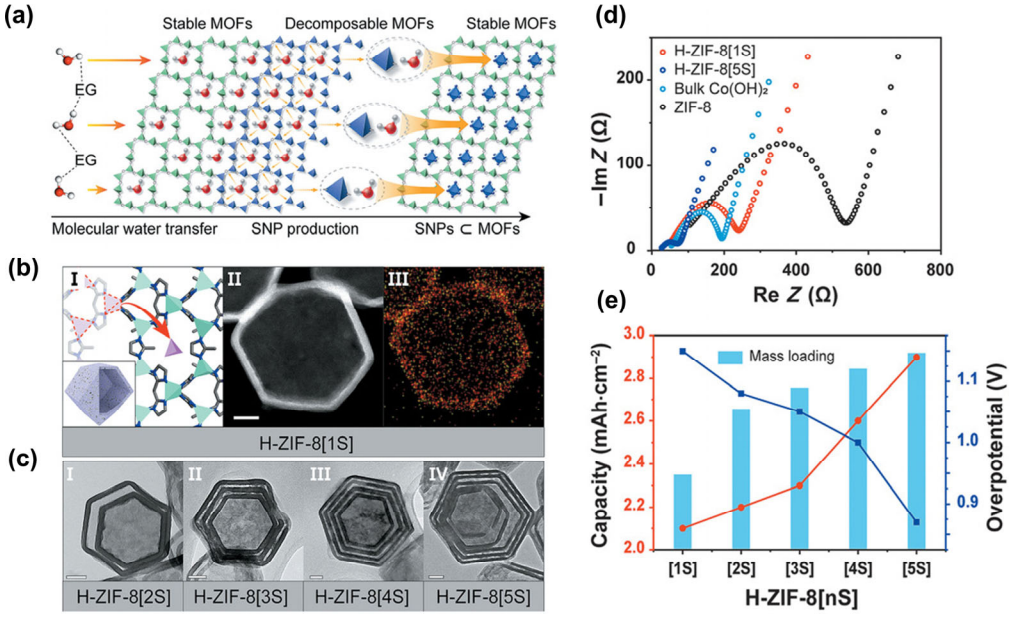

Figure 10 (a) Schematic of the formation process of SNP-embedded MOFs, where different colors signify different metal nodes. (b) I Illustrations of multishell with SNPs (green: Zn, violet: Co); II HAADF-STEM images of H-ZIF-8[1S]; III Elemental mapping images of H-ZIF-8[1S]. (c) TEM images of H-ZIF-8[2S, 3S, 4S, 5S]. All scale bars are 50 nm. (d) Nyquist plot corresponding to the EIS measurements conducted at 0.1–105 Hz with an amplitude of 10 mV. (e) Comparison plot of capacity and overpotential according to mass loading. Reproduced with permission from Ref. [102], © Choi, W. H. et al. 2020.

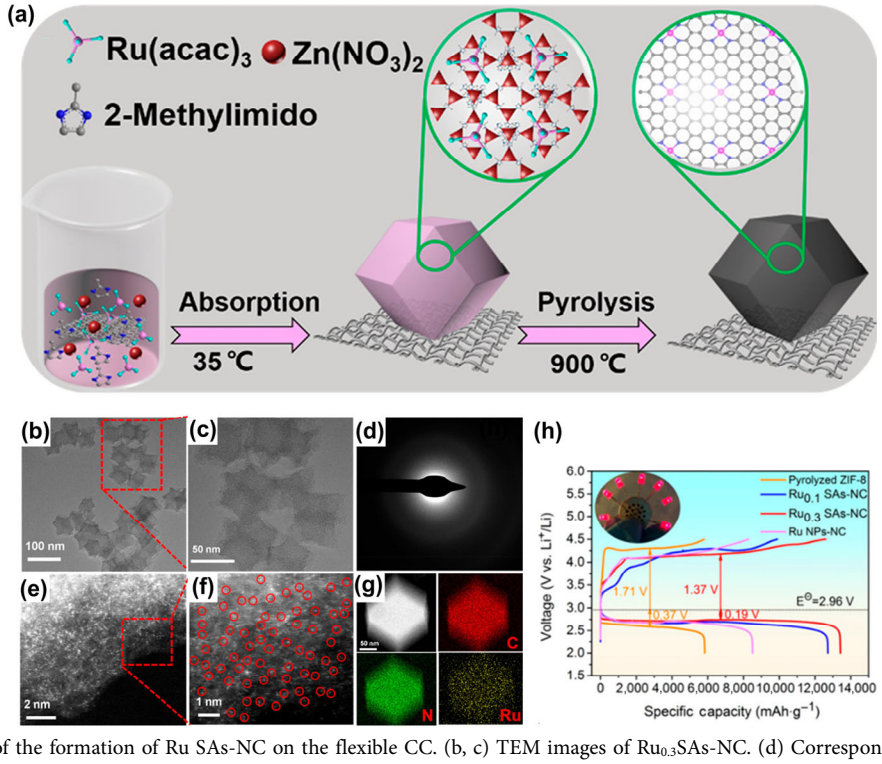

Figure 11 (a) Scheme of the formation of Ru SAs-NC on the flexible CC. (b, c) TEM images of $Ru_{0.3}$SAs-NC. (d) Corresponding SAED pattern of an individual rhombododecahedron. (e, f) HAADF-STEM images of $Ru_{0.3}$SAs-NC (Ru single atoms are marked with red circles). (g) Corresponding EDS maps revealing the homogeneous distribution of Ru and N within the carbon support of $Ru_{0.3}$SAs-NC. (h) The initial discharge-charge curves of LOBs with the four kinds of electrodes at a current density of 0.02 mA·cm^{-2}. Reproduced with permission from Ref. [103] © American Chemical Society 2020.

Archer's group reported a new type of Li-CO_2 battery operating at high temperature, which obtained the overall reaction is $4Li + 3CO_2 \leftrightarrow 2Li_2CO_3 + C$ [110]. Li's group realized the rechargeable Li-CO_2 battery at room temperature by using ($LiCF_3SO_3$)–TEGDME as electrolyte and the Li_2CO_3 and amorphous C as the main discharge products can be decomposed during charging [107]. Zhou's group used graphene as cathode for the first time in rechargeable Li-CO_2 batteries. Also noteworthy is the fact that Li_2CO_3 has crystal structure, which are more likely to detect than amorphous C. On the other hand, the ubiquitous of carbon materials in Li-CO_2 battery makes the source of amorphous C in discharge

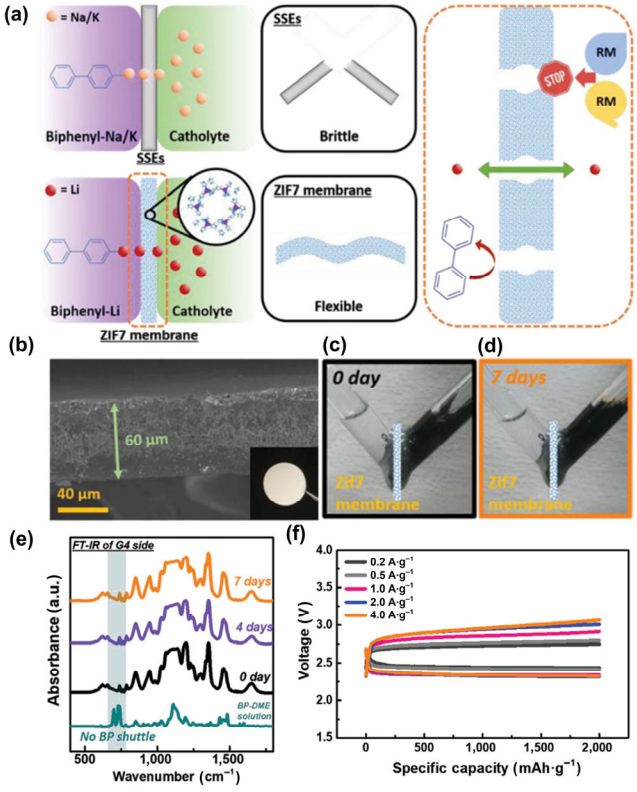

Figure 12 (a) Schematic illustration of the difference between the previous report of biphenyl-Na/K liquid anode with solid state electrolytes (SSEs) and this study of biphenyl-Li liquid anode with an ZIF-7 membrane separator. The proposed function of the ZIF-7 membrane in three aspects is also displayed. (b) The cross-side SEM images of the ZIF-7 membrane. Digital images of the permeation device (c) in the beginning (black) and (d) after 7 days (orange). (e) FT-IR spectra of the electrolytes extracted from the G4 side at different times. (f) Rate performances of the fabricated organic Li-O_2 batteries. Reproduced with permission from Ref. [106], © WILEY-VCH Verlag GmbH & Co. KGaA, Weinheim 2020.

products unclear. In order to confirm the existence of carbon, a platinum net rather than graphene was used as cathode for Li-CO_2 batteries [5]. The Pt net as cathode for the Li-CO_2 battery was discharged to 2.2 V. The results show a typical spectrum with a distinct edge of the K shell ionization energy characteristic of the corresponding carbon at 282 eV. Qiao *et al.* prepared gold as cathode for the Li-CO_2 battery to studied the variation trend of product types and components by *in-situ* surface-enhanced Raman spectroscopy [4]. Different from Li's group used ($LiCF_3SO_3$)-TEGDME, Qiao *et al.* used ($LiClO_4$)-DMSO as electrolyte due to the DMSO has high conductivity, low viscosity, and high CO_2 solubility. The surface of sputtered gold nanoparticles is rough, and its surface enhancement effect has stronger Raman peak signal. Additionally, the discharge products are $Li_2C_2O_4$ [111, 112] and HCOOH [113], respectively.

MOFs/COFs and their derivatives for Li-CO_2 battery

In 2018, Li *et al.* used MOFs as a catalyst of the cathode for Li-CO_2 battery for the first time [114]. Eight porous MOFs and two nonporous MOFs were studied in the Li-CO_2 batteries (Figs. 13(a)–13(f)). It was found that the MOFs with Mn sites could greatly reduce the charging overpotential, and the excellent CO_2 absorption capacity of MOFs tend to improve the discharge capacity. Furthermore, the MOFs with excellent CO_2 enrichment and the high dispersed metal catalytic active sites can further promote the decomposition of the products. *In-situ* DEMS results indicated that only CO_2 was produced in Mn_2(bobdc) electrode during recharging, which further demonstrated that the eversible reactions of $3CO_2$ + 4Li = $2Li_2CO_3$ + C take place on the MOFs. Lan's group designed the porphyrin-based two-dimensional MOFs of MnTPzP-Mn, CoTPzP-Mn, and CoTPzP-Co with dual-metal sites as the catalysts of the cathode for the Li-CO_2 batteries [115]. The metalloporphyrin can promote the activation of CO_2 and the metal-coordinated pyrazole can improved the complete efficient decomposition of product. Significantly, the MnTPzP-Mn as the catalyst of the cathode for the Li-CO_2 batteries shows a lower overpotential (1.05 V) and excellent cycle stability (90 cycles). Furthermore, Xu *et al.* prepared a Cu-tetra(4-carboxyphenyl) porphyrin (Cu-TCPP) nanosheets as cathode catalyst for Li-CO_2 batteries [116]. The Lewis base (−NH−) on the channel walls of the MOFs can produce strong interaction with acidic CO_2 gas [117]. The MOFs with high porosity and uniformly dispersed Cu-N_4 metal sites, provide suitable active sites and reaction space for the chemical conversion of CO_2. The polarization is only 1.8 V at 2,000 mA·g^{-1}.

Huang *et al.* designed the graphene@COF by using imide COF is uniformly covering the graphene as catalyst of the cathode for the Li-CO_2 batteries [118]. CO_2 can be enriched and confined in the micropores of the Imine-COF. On the one hand, the enrichment and confinement effects optimize the diffusion path of CO_2 and enhances the conductivity of electrons and lithium ions. On the other hand, the regular structure fragments of COFs can avoid the accumulation of a large number of discharge products caused by high CO_2 concentration. In addition, Li *et al.* prepared a composite material by combining hydrazine-linked COF and CNT coated with Ru nanoparticles (COF-Ru@CNT) as an efficient catalyst (Fig. 14(a)) [119]. The COFs can markedly improve the ability of capturing CO_2 in discharge process and promote the decomposition of product during recharging. In addition, the unique pore structure of COFs can be used as a diffusion layer for Li^+ and CO_2, thus enhancing the rate performance (Figs. 14(b) and 14(c)). The Li-CO_2 batteries with COF-based catalysts have an excellent rate performance and operated stably for 200 cycles at current density of 1,000 mA·g^{-1} with no significant voltage decay during charging and discharging processes (Figs. 14(d)–14(g)). Recently, researchers have noted that the combination of tetrathiafulvalene (TTF) as electron donor with metalloporphyrin as electron acceptor to prepared COFs, which can increase the electron efficiency and speed up the transfer of the intermolecular charge-electron [120]. Lan's group designed a porphyrin-based COFs with Mn single atom sites (TTCOF-Mn) and found that: (i) The uniformly distributed porphyrin centers are enrich in Mn-N_X sites, which are beneficial to the catalytic activation process of CO_2. (ii) The combination of the metal center with the electron-donating ligand can effectively realize the intramolecular electron transport. (iii) It has the porous, large specific surface area and stable chemical properties, which can ensure the key steps of reaction such as active gas adsorption, uniform ion dispersion and rapid mass transfer can be carried out effectively in the Li-CO_2 batteries [121].

2.5 Sodium-air batteries

Sodium as anode for air batteries has great potential because of the moderate cost, abundant reserves, and relatively high

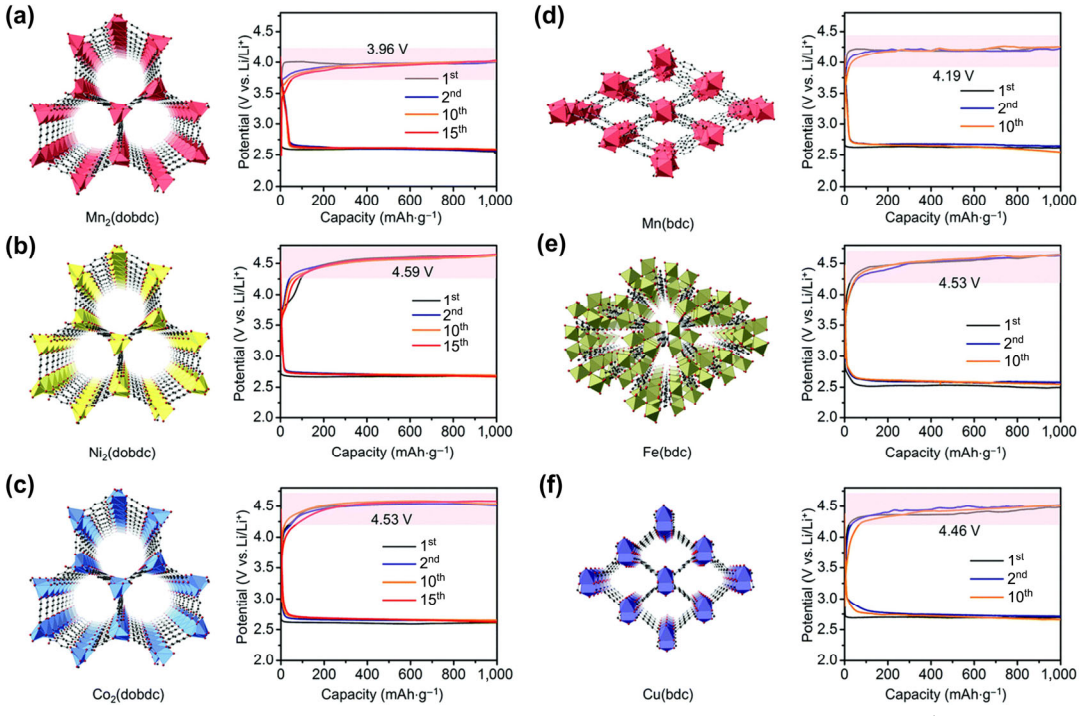

Figure 13 Crystal of (a–c) M_2(dobdc) and (d–f) M(bdc), and their corresponding discharge-charge curves at 50 mA·g^{-1}. Reproduced with permission from Ref. [114], © The Royal Society of Chemistry 2018.

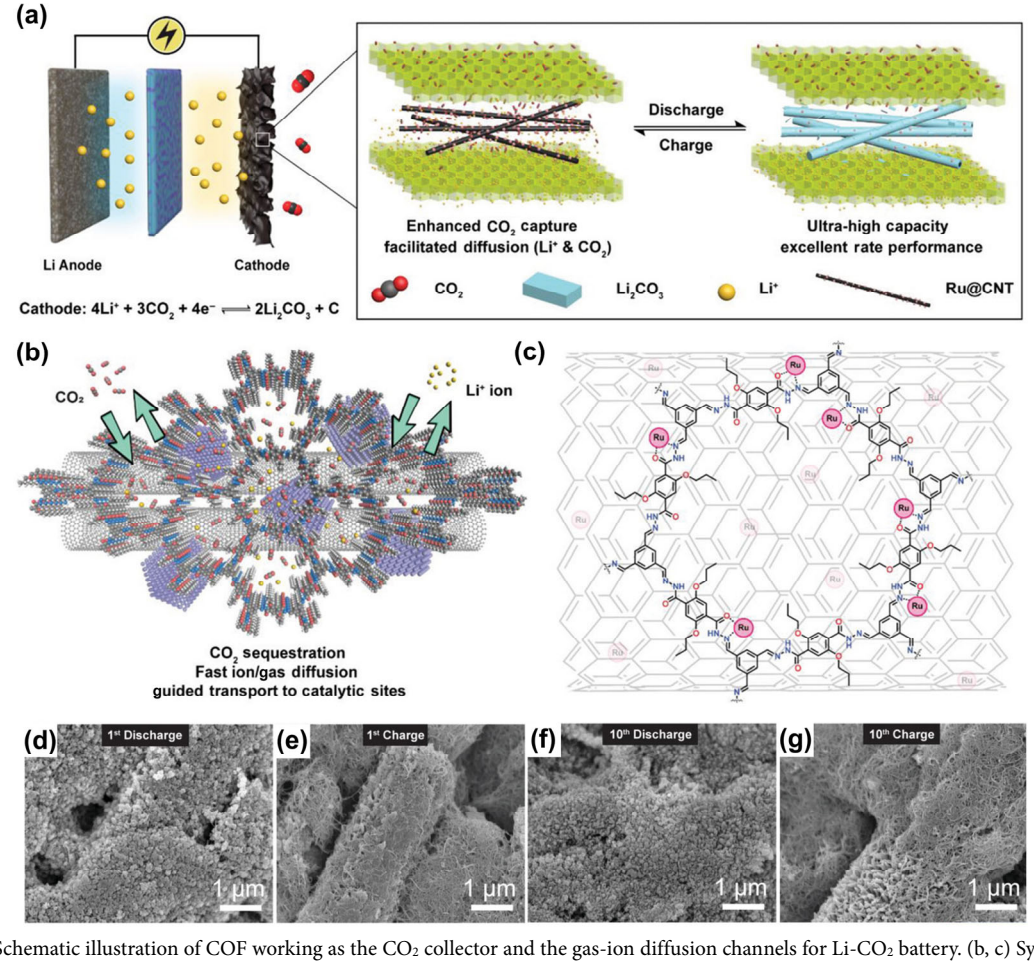

Figure 14 (a) Schematic illustration of COF working as the CO_2 collector and the gas-ion diffusion channels for Li-CO_2 battery. (b, c) Synthesis of highly crystalline Tf-DHzOPr COF interfaced with Ru@CNT via hydrazide-metal coordination. SEM images of COF-Ru@CNT after (d) first discharge, (e) first charge, (f) tenth discharge, and (g) tenth charge. Reproduced with permission from Ref. [119] © WILEY-VCH Verlag GmbH & Co. KGaA, Weinheim 2019.

electrode potential (–2.71 V vs. SHE) [122, 123]. The sodium-air (Na-air) batteries with high energy density of 1,683 Wh·kg^{-1}, which is calculated from $2Na^+ + O_2 + 2e^- \leftrightarrow Na_2O$ [124]. The ORR and OER processes with slow kinetics during discharging and recharging, which involves complex multielectron three-phase interfacial reactions and eventually leads to large polarization for the Na-air batteries.

Peled *et al.* first reported a liquid Na-air batteries based on the polymer electrolyte at 100 °C [125]. However, liquid sodium is highly corrosive and the high temperature condition is inconvenient for practical application. Therefore, Fu *et al.* reported a non-aqueous Na-air batteries with diamond-like film as the cathode at room temperature and the 1 M $NaPF_6$ dissolve in ethylene carbonate and dimethyl carbonate as electrolytes [126]. The Na-O_2 batteries at room-temperature achieves a high reversible capacity and discharge platform of up to 2.3 V. Furthermore, the crystalline Na_2O_2 is found in the discharge products. The mechanism of charge and discharge reactions are as follows:

Anode: $2Na \leftrightarrow 2Na^+ + 2e^-$

Cathode: $2Na^+ + O_2 + 2e^- \leftrightarrow Na_2O_2$

$$n Na^+ + O_2 + EC/DEC + ne^- \leftrightarrow Na_2CO_3 + NaOCO\text{-}R + \text{side products}$$

$$2Na_2O_2 + 2CO_2 \leftrightarrow 2Na_2O_2$$

Hartmann *et al.* reported a rechargeable Na-O_2 batteries at room temperature, and the cubic particle NaO_2 is the main discharge product [127]. Apart from that, Hartmann *et al.* realized a reversible Na-O_2 battery at room temperature by using pure carbon materials as cathode [128]. The solid discharge product of crystalline NaO_2 is formed in a one-electron transfer step.

Archer's group reported a novel tetraglyme-based Na-CO_2/O_2 batteries at room temperature [129]. In addition, Archer's group design a rechargeable Na-CO_2/O_2 batteries utilizes the SiO_2-IL-TFSI/PC-NaTFSI hybrid electrolyte. The XRD results indicate that the main discharge product is $NaHCO_3$, which was decomposed to CO_2 and a small amount of O_2 during recharging process [130]. The probably mechanism of Na-O_2/CO_2 batteries are as follows [130]:

$$Na + 1/2H_2 + CO_2 + 1/2O_2 \rightarrow NaHCO_3 \quad E^\theta = 2.88 \text{ V (vs. Na/Na}^+\text{)}$$

MOFs and their derivatives for Na-air battery

In 2019, Wu *et al.* firstly prepared N-doped carbon nanotubes derived from ZIF-67 MOFs (MOF-NCNTs) as catalyst for the hybrid Na-air batteries (Fig. 15(a)) [131]. ZIF-67 particles can provide carbon source for catalyze the further growth of cobalt nanoparticles for carbon nanotubes during the heat treatment process (Figs. 15(b)–15(e)) [132, 133]. Significantly, the excellent electrochemical performance is due to the synergistic effect between N and confined Co nanoparticles in carbon nanotubes, which promotes the electron transfer in ORR and OER processes. What's more, the hollow structure and robust porous cage derived from MOFs can promote the

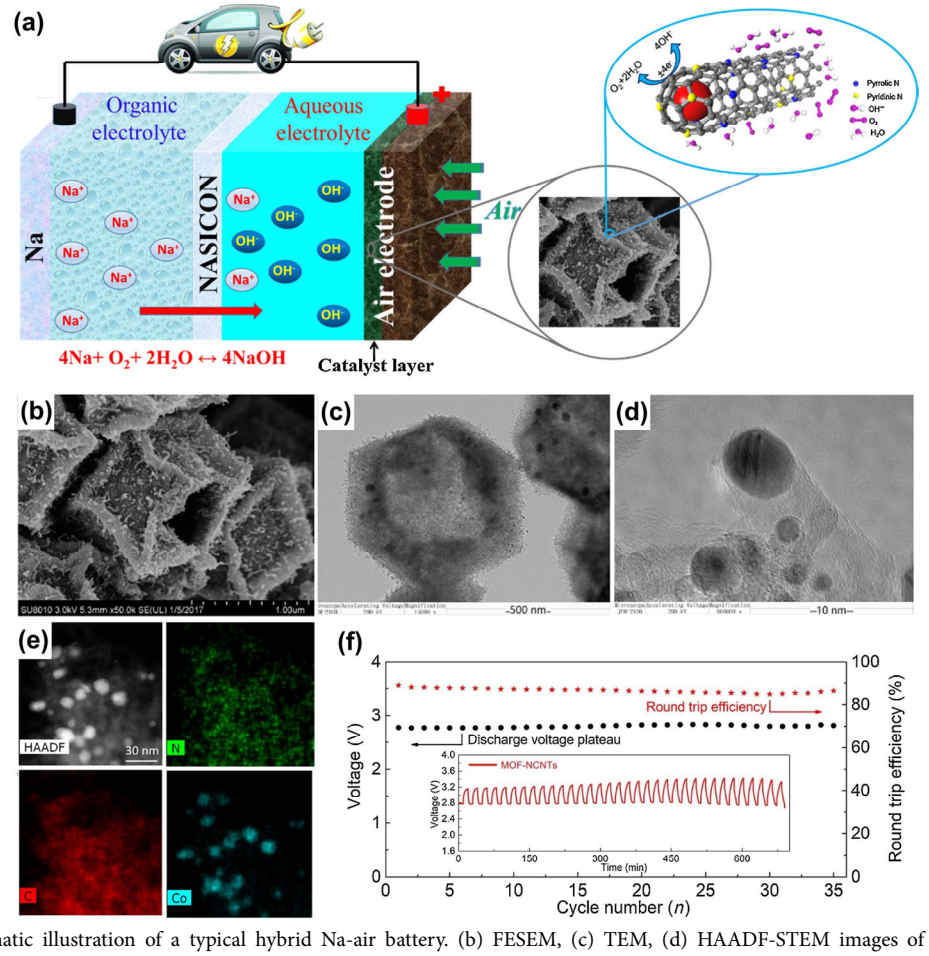

Figure 15 (a) Schematic illustration of a typical hybrid Na-air battery. (b) FESEM, (c) TEM, (d) HAADF-STEM images of MOF-NCNTs, (e) the corresponding element mapping of C, N, and Co. (f) Cycling performance of hybrid Na-air batteries with MOF-NCNTs as catalyst at 0.1 mA·cm^{-2}. Reproduced with permission from Ref. [131], © Elsevier B.V. 2019.

O_2 adsorption and the proton transportation, leading to the excellent stability of electrocatalysis for the Na-air batteries. And then, the Na-air battery with MOF-NCNTs has lower overpotential is 0.3 V at current density of 100 $mA \cdot g^{-1}$ (Fig. 15(f)). Particularly, because of the bimetal organic framework derived hybrid materials have the porous structure and gas adsorption capacity, exhibiting excellent ORR catalytic activity in recent year. Subsequently, Zhu *et al.* reported a N-doped defective carbon nano-framework with cobalt nanoparticles derived from ZnCo bimetal MOFs (Co-N-C) as catalyst for the hybrid Na-air battery [134]. The Co-N-C with high specific surface area is ascribe to the evaporation of zinc, which facilitates the adsorption and desorption of oxygen and also provides a large number of catalytic sites [135]. The synergistic catalytic effect between nitrogen-doped carbon and Co opens up a new way to develop the bifunctional catalysts for ORR/OER.

Due to the bad thermal stability, low efficiency of active site and poor conductivity at the interface of directly carbonized MOFs, more and more studies tend to regulate the active sites on the basis of the MOFs-derivates to meet the standard of the practical applications. Other than that, the different types of MOFs make it possible to prepare a variety of MOFs-derived nanocomposites. There is no doubt that the MOFs have great potential in Na-air batteries as the preferred material for the preparation of carbon nanocomposites.

2.6 Aluminum-air batteries

In 1962, Zaromb firstly proposed the use of aluminium metal anodes with high energy density in aluminium/oxygen systems [136, 137]. The aluminum-air (Al-air) batteries have a theoretical energy density of 8,000 $Wh \cdot kg^{-1}$ and great application value in electric vehicle and submarine power supply [138]. The mechanism of charge and discharge reactions are as follows [137].

Anode: $Al - 3e^- \rightarrow Al^{3+}$
Cathode: $O_2 + 2H_2O + 2e^- \rightarrow 4OH^-$
Overall reaction: $Al + 3O_2 + 6H_2O \leftrightarrow 4Al(OH)_3 \quad (U^0 = 2.74\ V)$

The Al-air batteries system is an excellent electrochemical storage system with a high energy density, making it an attractive candidate for electric vehicle.

MOFs and their derivatives for Al-air battery

To obtain the chemical stability of MOFs-based catalysts, we often convert primitive MOFs into metal oxide/carbon composites. Li *et al.* first reported a catalyst containing Cu/Cu_2O nanoparticles and amorphous CuN_xC_y in the Al-air batteries (Fig. 16(a)) [139]. The hybrid catalyst obtained by using Cu-MOF as a sacrifice template to modify Ketjenblack carbon, which could be used as active sites to accelerate

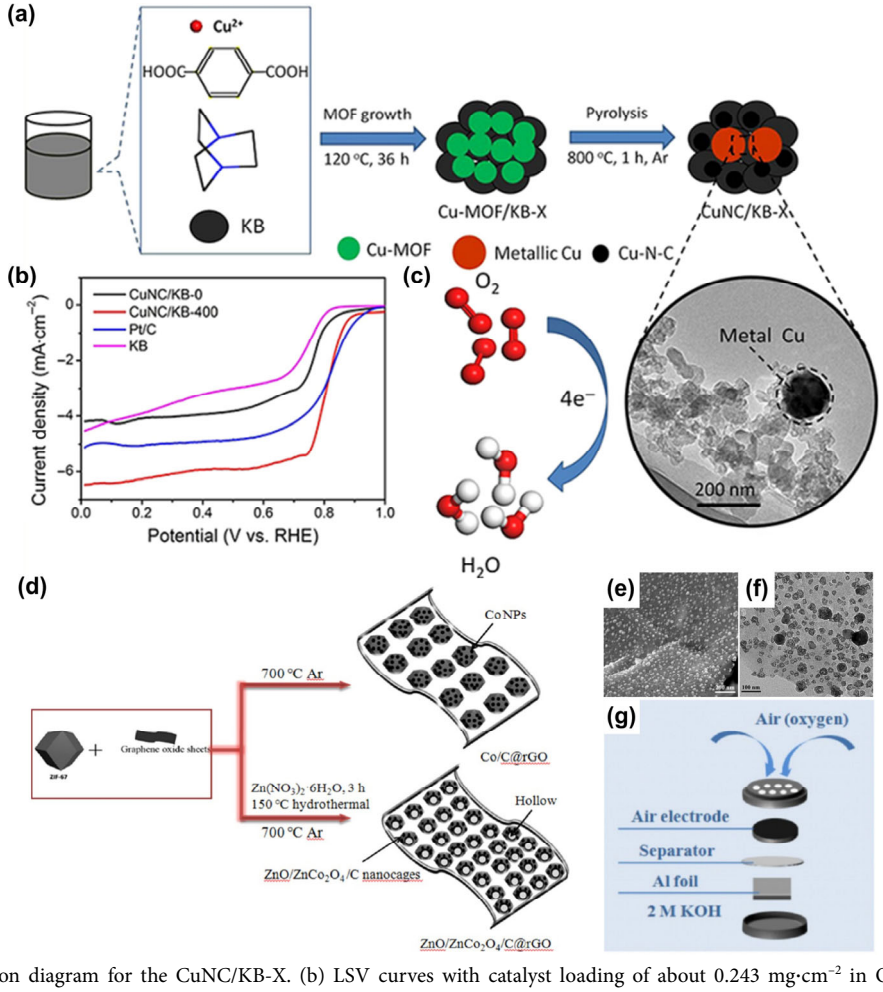

Figure 16 (a) Preparation diagram for the CuNC/KB-X. (b) LSV curves with catalyst loading of about 0.243 $mg \cdot cm^{-2}$ in O_2-saturated 0.1 M KOH. (c) Diagram of reaction mechanism. (a)-(c) Reproduced with permission from Ref. [139] © The Royal Society of Chemistry 2017. (d) Schematic illustration for the synthesis of Co/C@rGO and $ZnO/ZnCo_2O_4$/C@rGO. (e) SEM and (f) TEM images of the $ZnO/ZnCo_2O_4$/C@rGO. (g) Conformation of a coin Al-air cell. Reproduced with permission from Ref. [140], © American Chemical Society 2017.

the ORR process (Figs. 16(b) and 16(c)). Liu *et al.* designed the $ZnO/ZnCo_2O_4$/C@rGO as cathode for Al-air batteries, which derived from zeolitic imidazolate framework (ZIF-67) (Fig. 16(d)) [140]. On the one hand, the MOFs-derived nanostructures have the characteristics of large surface area, robust morphology and porosity, which become the promising ORR electrocatalysts. On the other hand, the rGO has good electrical properties, large specific surface area and favourable mechanical strength. The resultant composites have high conductivity, dispersion and chemical stability (Figs. 16(e) and 16(f)). Hence, the unique nanocage structure and the cooperative covalent coupling between highly conductive rGO can induce high dispersion, excellent chemical stability, and more catalytic active sites. Furthermore, a new type of simple primary coin Al-air battery was firstly prepared in order to further explore the actual electrochemical performance (Fig. 16(g)).

The greatest advantage of MOFs is its highly adjustable and structured channel, which allows the material composition and structure to be designed and optimized according to the requirements of the Al-air batteries system. Therefore, it is necessary to develop low-cost and efficient MOFs-based catalysts, but it is still challenging to achieve practical applications.

3 Perspective and outlook

Recently, the researches of MOFs and COFs in the metal-air batteries have shown exponential growth due to their high specific surface area, porosity, pore size and control of components. On the one hand, their functional porous walls can produce strong adsorption with CO_2 and O_2. On the other hand, adsorption near the catalytic site can significantly improve the catalytic efficiency. The pore size of MOFs and COFs are not only to satisfy the rapid transportation of gases, electrolyte and the intermediate species, but also to meet the requirement that the distance between adsorption and catalytic sites is not be too far away, which should select the different ligands to optimize the pore size to improve the catalytic efficiency. Consequently, the unique advantages of MOFs and COFs are shorter diffusion paths, easier access to active sites for surface reactions, and diversity of functionalization with other inorganic components. Additionally, the unique molecular structure of MOFs and COFs enables them to maintain high porosity while ensuring uniform distribution of catalytic sites, which is different from other materials with pore structure. Although MOFs and COFs are both crystalline porous materials with wide application prospects, their respective inherent limitations limit their application to a certain extent. The use of MOFs in electrochemistry is limited by its inherent poor electrical conductivity and relatively unstable structure through coordination bonds. As for COFs, the limitations are that they have no metal nodes and relatively simple functions, and their catalytic performance needs to be further improved. Then, I will put forward my own views on the applications of COFs and MOFs in the field of energy storage and conversion.

First and foremost, in view of the complexity of the batteries system, it is necessary to systematically study the effects between the organic ligands and the catalytic active centers of MOFs and COFs. On the one hand, it can provide a theoretical basis for us to select and synthesize the desired MOFs and COFs catalysts in the future. On the other hand, it is helpful to have a deeper understanding of the local microenvironment in MOFs and COFs on the overall catalytic effect. At present, the application of MOFs and COFs in other metal-air battery systems described in this review, such as Mg-air, K-air, Fe-air, and Li-N_2 batteries is almost non-existent. In the Li-N_2 batteries, particularly, we can realize that under mild conditions only electricity and N_2 as feedstock to fix N_2. Although the N_2 obtained from the atmosphere is unlimited, due to the N_2 with strong non-polar N≡N covalent triple bond energy and high ionization energy [141], making the low energy efficiency of Li-N_2 batteries is also a common problem. Therefore, the preparation of functionalized MOFs and COFs based on the reaction mechanism of metal-air batteries is also a promotion for the development of novel metal-air batteries in the future.

Secondly, as I mentioned before, it can be seen that the hybrid of MOFs and COFs show stronger functions and properties than the original single MOFs or COFs [75]. Therefore, among various hybrid strategies, MOF-COF hybrid materials are of great application potential and research value. We can design MOF-COF hybrid materials with both excellent catalytic performance of MOFs unsaturated coordination metal center and high chemical stability brought by COFs covalent bonding for application in the field of energy storage. It should be noted that the low intrinsic conductivity of MOFs and COFs is an important limiting factor for their use as efficient electrocatalysts. Therefore, the conductivity can be significantly improved through the combination of electron good conductors, pyrolysis and doping strategies. In addition, the unique electron delocalization effect in MOFs makes the motion range of π electron no longer limited, and further electron migration between active sites can significantly promote the catalytic activity of chemical reactions and enhance electron conductivity.

Additionally, though the MOF and COF-derivatives have been widely used in the batteries, the composition control and morphology retention in the conversion process are still in the early stages. Therefore, I think that precise control of material structure design is the key to achieve high efficiency electrocatalytic performance. For the structural regulation of pure MOFs and COFs, the local microenvironment can be regulated through the change of ligands and metal sites. Barthram *et al.* showed that 2,3,6,7,10, 11-hexahydroxytriphenyl ($H_{12}C_{18}O_6$, HHTP) is a redox active linker, which has a reversible conversion between catecholates, semiquinonate and quinones [142]. Therefore, in 2012, Yaghi's group successfully prepared a Cu-CAT-1 (Cu-HHTP) crystalline material with high chemical stability, porosity and excellent electrical conductivity [143]. The reversible transformation of Cu^+/Cu^{2+} shows that it has a good application prospect in the energy storage [144]. Composite materials of MOFs and COFs can be prepared by encapsulation, coating or sandwich with MOFs and COFs [145,146], which can effectively avoid the disadvantages of low conductivity and poor catalytic effect of single-component materials. What's more, rational modeling and theoretical calculations also provide important reference values for understanding the relationship between complex nanostructured of MOFs and COFs-derivatives and electrochemical properties.

In the end, the advances of *in-situ* characterization techniques are helpful to understand the catalytic mechanism and redox reaction processes of MOFs and COFs in the metal-air batteries. In spite of this, the metal-air batteries generally involve the reaction at the three-phase interface, and it is difficult to accurately determine the critical catalytic role of MOFs and COFs in the testing process. Therefore, the development of the *in-situ* detection with the advanced

techniques is essential to fully reveal the relationship between the structure and the performance. During the operation of the battery, *in-situ* Surface-Enhanced Raman Scattering (SERS) and Infrared Radiation (IR) spectrum can record the vibration signal of molecules on the electrode surface and observe the conversion process of intermediate state products. Other than that, the Differential Electrochemical Mass Spectrometry (DEMS) can monitor volatile gas products and kinetic parameters. These *in-situ* testing methods can provide important experimental and theoretical basis for guiding catalyst design and optimizing reaction conditions to regulate reaction performance.

Acknowledgements

The authors thank for the financial support from the National Defense Technology Innovation Special Zone Spark Project (No. 2016300TS00911901), the Natural Science Foundation of Jiangsu Province (No. BK20210616), and a Project Funded by the Priority Academic Program Development of Jiangsu Higher Education Institutions (PAPD).

Declaration of conflicting interests

The authors declare no conflicting interests regarding the content of this article.

References

[1] Nejat, P.; Jomehzadeh, F.; Taheri, M. M.; Gohari, M.; Majid, M. Z. A. A global review of energy consumption, CO_2 emissions and policy in the residential sector (with an overview of the top ten CO_2 emitting countries). *Renew. Sust. Energy Rev.* **2015**, *43*, 843–862.

[2] Kélouwani, S.; Agbossou, K.; Chahine, R. Model for energy conversion in renewable energy system with hydrogen storage. *J. Power Sources* **2005**, *140*, 392–399.

[3] Fu, G. T.; Chen, Y. F.; Cui, Z. M.; Li, Y. T.; Zhou, W. D.; Xin, S.; Tang, Y. W.; Goodenough, J. B. Novel hydrogel-derived bifunctional oxygen electrocatalyst for rechargeable air cathodes. *Nano Lett.* **2016**, *16*, 6516–6522.

[4] Qiao, Y.; Yi, J.; Wu, S. C.; Liu, Y.; Yang, S. X.; He, P.; Zhou, H. S. Li-CO_2 electrochemistry: A new strategy for CO_2 fixation and energy storage. *Joule* **2017**, *1*, 359–370.

[5] Zhang, Z.; Zhang, Q.; Chen, Y. N.; Bao, J.; Zhou, X. L.; Xie, Z. J.; Wei, J. P.; Zhou, Z. The first introduction of graphene to rechargeable Li-CO_2 batteries. *Angew. Chem., Int. Ed.* **2015**, *54*, 6550–6553.

[6] Wen, X. D.; Zhang, Q. Q.; Guan, J. Q. Applications of metal-organic framework-derived materials in fuel cells and metal-air batteries. *Coord. Chem. Rev.* **2020**, *409*, 213214.

[7] Cui, Z. M.; Fu, G. T.; Li, Y. T.; Goodenough, J. B. Ni_3FeN-supported Fe_3Pt intermetallic nanoalloy as a high-performance bifunctional catalyst for metal-air batteries. *Angew. Chem., Int. Ed.* **2017**, *56*, 9901–9905.

[8] Rosi, N. L.; Eddaoudi, M.; Kim, J.; O'Keeffe, M.; Yaghi, O. M. Infinite secondary building units and forbidden catenation in metal-organic frameworks. *Angew. Chem., Int. Ed.* **2002**, *41*, 284–287.

[9] Furukawa, H.; Ko, N.; Go, Y. B.; Aratani, N.; Choi, S. B.; Choi, E.; Yazaydin, A. Ö.; Snurr, R. Q.; O'Keeffe, M.; Kim, J. et al. Ultrahigh porosity in metal-organic frameworks. *Science* **2010**, *329*, 424–428.

[10] Millward, A. R.; Yaghi, O. M. Metal-organic frameworks with exceptionally high capacity for storage of carbon dioxide at room temperature. *J. Am. Chem. Soc.* **2005**, *127*, 17998–17999.

[11] Park, K. S.; Ni, Z.; Côté, A. P.; Choi, J. Y.; Huang, R. D.; Uribe-Romo, F. J.; Chae, H. K.; O'Keeffe, M.; Yaghi, O. M. Exceptional chemical and thermal stability of zeolitic imidazolate frameworks. *Proc. Natl. Acad. Sci. USA* **2006**, *103*, 10186–10191.

[12] Dang, Y. T.; Hoang, H. T.; Dong, H. C.; Bui, K. B. T.; Nguyen, L. H. T.; Phan, T. B.; Kawazoe, Y.; Doan, T. L. H. Microwave-assisted synthesis of nano Hf-and Zr-based metal-organic frameworks for enhancement of curcumin adsorption. *Micropor. Mesopor. Mater.* **2020**, *298*, 110064.

[13] Cavka, J. H.; Jakobsen, S.; Olsbye, U.; Guillou, N.; Lamberti, C.; Bordiga, S.; Lillerud, K. P. A new zirconium inorganic building brick forming metal organic frameworks with exceptional stability. *J. Am. Chem. Soc.* **2008**, *130*, 13850–13851.

[14] Bourrelly, S.; Llewellyn, P. L.; Serre, C.; Millange, F.; Loiseau, T.; Férey, G. Different adsorption behaviors of methane and carbon dioxide in the isotypic nanoporous metal terephthalates MIL-53 and MIL-47. *J. Am. Chem. Soc.* **2005**, *127*, 13519–13521.

[15] Xie, X. Y.; Peng, L. S.; Yang, H. Z.; Waterhouse, G. I. N.; Shang, L.; Zhang, T. R. MIL-101-derived mesoporous carbon supporting highly exposed Fe single-atom sites as efficient oxygen reduction reaction catalysts. *Adv. Mater.* **2021**, *33*, 2101038.

[16] Côté, A. P.; Benin, A. I.; Ockwig, N. W.; O'Keeffe, M.; Matzge, A. J.; Yaghi, O. M. Porous, crystalline, covalent organic frameworks. *Science* **2005**, *310*, 1166–1170.

[17] Uribe-Romo, F. J.; Doonan, C. J.; Furukawa, H.; Oisaki, K.; Yaghi, O. M. Crystalline covalent organic frameworks with hydrazone linkages. *J. Am. Chem. Soc.* **2011**, *133*, 11478–11481.

[18] Hunt, J. R.; Doonan, C. J.; LeVangie, J. D.; Côté, A. P.; Yaghi, O. M. Reticular synthesis of covalent organic borosilicate frameworks. *J. Am. Chem. Soc.* **2008**, *130*, 11872–11873.

[19] Fang, Q. R.; Zhuang, Z. B.; Gu, S.; Kaspar, R. B.; Zheng, J.; Wang, J. H.; Qiu, S. L.; Yan, Y. S. Designed synthesis of large-pore crystalline polyimide covalent organic frameworks. *Nat. Commun.* **2014**, *5*, 4503.

[20] Du, Y.; Yang, H. S.; Whiteley, J. M.; Wan, S.; Jin, Y. H.; Lee, S. H.; Zhang, W. Ionic covalent organic frameworks with spiroborate linkage. *Angew. Chem., Int. Ed.* **2016**, *55*, 1737–1741.

[21] Diercks, C. S.; Yaghi, O. M. The atom, the molecule, and the covalent organic framework. *Science* **2017**, *355*, eaal1585.

[22] Zhang, Y. Y.; Duan, J. Y.; Ma, D.; Li, P. F.; Li, S. W.; Li, H. W.; Zhou, J. W.; Ma, X. J.; Feng, X.; Wang, B. Three-dimensional anionic cyclodextrin-based covalent organic frameworks. *Angew. Chem., Int. Ed.* **2017**, *56*, 16313–16317.

[23] Uribe-Romo, F. J.; Hunt, J. R.; Furukawa, H.; Klöck, C.; O'Keeffe, M.; Yaghi, O. M. A crystalline imine-linked 3D porous covalent organic framework. *J. Am. Chem. Soc.* **2009**, *131*, 4570–4571.

[24] Geng, K. Y.; He, T.; Liu, R. Y.; Dalapati, S.; Tan, K. T.; Li, Z. P.; Tao, S. S.; Gong, Y. F.; Jiang, Q. H.; Jiang, D. L. Covalent organic frameworks: Design, synthesis, and functions. *Chem. Rev.* **2020**, *120*, 8814–8933.

[25] Sudik, A. C.; Millward, A. R.; Ockwig, N. W.; Côté, A. P.; Kim, J.; Yaghi, O. M. Design, synthesis, structure, and gas (N_2, Ar, CO_2, CH_4, and H_2) sorption properties of porous metal-organic tetrahedral and heterocuboidal polyhedra. *J. Am. Chem. Soc.* **2005**, *127*, 7110–7118.

[26] Rowsell, J. L. C.; Spencer, E. C.; Eckert, J.; Howard, J. A. K.; Yaghi, O. M. Gas adsorption sites in a large-pore metal-organic framework. *Science* **2005**, *309*, 1350–1354.

[27] Furukawa, H.; Cordova, K. E.; O'Keeffe, M.; Yaghi, O. M. The chemistry and applications of metal-organic frameworks. *Science* **2013**, *341*, 1230444.

[28] Yaghi, O. M.; O'Keeffe, M.; Ockwig, N. W.; Chae, H. K.; Eddaoudi, M.; Kim, J. Reticular synthesis and the design of new materials. *Nature* **2003**, *423*, 705–714.

[29] Xia, Q.; Wang, H.; Huang, B. B.; Yuan, X. Z.; Zhang, J. J.; Zhang, J.; Jiang, L. B.; Xiong, T.; Zeng, G. M. State-of-the-art advances and challenges of iron-based metal organic frameworks from attractive features, synthesis to multifunctional applications. *Small* **2019**, *15*, 1803088.

[30] Liu, J. W.; Xie, D. X.; Shi, W.; Cheng, P. Coordination compounds in lithium storage and lithium-ion transport. *Chem. Soc. Rev.* **2020**, *49*, 1624–1642.

[31] Zhang, L.; Liu, H. W.; Shi, W.; Cheng, P. Synthesis strategies and potential applications of metal-organic frameworks for electrode materials for rechargeable lithium ion batteries. *Coord. Chem. Rev.* **2019**, *388*, 293–309.

[32] Liu, J. W.; Xie, D. X.; Xu, X. F.; Jiang, L. Z.; Si, R.; Shi, W.; Cheng, P. Reversible formation of coordination bonds in Sn-based metal-organic frameworks for high-performance lithium storage. *Nat. Commun.* **2021**, *12*, 3131.
[33] Huang, N. Y.; He, H.; Liu, S. J.; Zhu, H. L.; Li, Y. J.; Xu, J.; Huang, J. R.; Wang, X.; Liao, P. Q.; Chen, X. M. Electrostatic attraction-driven assembly of a metal-organic framework with a photosensitizer boosts photocatalytic CO_2 reduction to CO. *J. Am. Chem. Soc.* **2021**, *143*, 17424–7430.
[34] Paz, F. A. A.; Klinowski, J.; Vilela, S. M. F.; Tomé, J. P. C.; Cavaleiro, J. A. S.; Rocha, J. Ligand design for functional metal-organic frameworks. *Chem. Soc. Rev.* **2012**, *41*, 1088–1110.
[35] Schoedel, A.; Ji, Z.; Yaghi, O. M. The role of metal-organic frameworks in a carbon-neutral energy cycle. *Nat. Energy* **2016**, *1*, 16034.
[36] Zhang, H. B.; Nai, J. W.; Yu, L.; Lou, X. W. Metal-organic-framework-based materials as platforms for renewable energy and environmental applications. *Joule* **2017**, *1*, 77–107.
[37] Zhu, B. J.; Liang, Z. B.; Xia, D. G.; Zou, R. Q. Metal-organic frameworks and their derivatives for metal-air batteries. *Energy Storage Mater.* **2019**, *23*, 757–771.
[38] Eddaoudi, M.; Kim, J.; Rosi, N.; Vodak, D.; Wachter, J.; O'Keeffe, M.; Yaghi, O. M. Systematic design of pore size and functionality in isoreticular MOFs and their application in methane storage. *Science* **2002**, *295*, 469–472.
[39] Banerjee, R.; Phan, A.; Wang, B.; Knobler, C.; Furukawa, H.; O'Keeffe, M.; Yaghi, O. M. High-throughput synthesis of zeolitic imidazolate frameworks and application to CO_2 capture. *Science* **2008**, *319*, 939–943.
[40] Banerjee, R.; Furukawa, H.; Britt, D.; Knobler, C.; O'Keeffe, M.; Yaghi, O. M. Control of pore size and functionality in isoreticular zeolitic imidazolate frameworks and their carbon dioxide selective capture properties. *J. Am. Chem. Soc.* **2009**, *131*, 3875–3877.
[41] Zlotea, C.; Campesi, R.; Cuevas, F.; Leroy, E.; Dibandjo, P.; Volkringer, C.; Loiseau, T.; Férey, G.; Latroche, M. Pd nanoparticles embedded into a metal-organic framework: Synthesis, structural characteristics, and hydrogen sorption properties. *J. Am. Chem. Soc.* **2010**, *132*, 2991–2997.
[42] Varela, A. S.; Ju, W.; Bagger, A.; Franco, P.; Rossmeisl, J.; Strasser, P. Electrochemical reduction of CO_2 on metal-nitrogen-doped carbon catalysts. *ACS Catal.* **2019**, *9*, 7270–7284.
[43] Li, X. N.; Liu, L. H.; Ren, X. Y.; Gao, J. J.; Huang, Y. Q.; Liu, B. Microenvironment modulation of single-atom catalysts and their roles in electrochemical energy conversion. *Sci. Adv.* **2020**, *6*, abb6833.
[44] Ji, D. X.; Fan, L.; Li, L. L.; Peng, S. J.; Yu, D. S.; Song, J. N.; Ramakrishna, S.; Guo, S. J. Atomically transition metals on self-supported porous carbon flake arrays as binder-free air cathode for wearable zinc-air batteries. *Adv. Mater.* **2019**, *31*, 1808267.
[45] Côté, A. P.; El-Kaderi, H. M.; Furukawa, H.; Hunt, J. R.; Yaghi, O. M. Reticular synthesis of microporous and mesoporous 2D covalent organic frameworks. *J. Am. Chem. Soc.* **2007**, *129*, 12914–12915.
[46] Lyu, H.; Diercks C, S.; Zhu, C. H.; Yaghi, O. M. Porous crystalline olefin-linked covalent organic frameworks. *J. Am. Chem. Soc.* **2019**, *141*, 6848–6852.
[47] Wan, S.; Guo, J.; Kim, J.; Ihee, H.; Jiang, D. L. A belt-shaped, blue luminescent, and semiconducting covalent organic framework. *Angew. Chem., Int. Ed.* **2008**, *47*, 8826–8830.
[48] Waller, P. J.; Gándara, F.; Yaghi, O. M. Chemistry of covalent organic frameworks. *Acc. Chem. Res.* **2015**, *48*, 3053–3063.
[49] Gottschling K.; Savasci G.; Vignolo-González H.; Schmidt S.; Mauker P.; Banerjee T.; Rovó P.; Ochsenfeld C.; Lotsch B. V. Rational design of covalent cobaloxime-COF hybrids for enhanced photocatalytic hydrogen evolution. *J. Am. Chem. Soc.* **2020**, *142*, 12146–12156.
[50] Dalapati, S.; Jin, S. B.; Gao, J.; Xu, Y. H.; Nagai, A.; Jiang, D. L. An azine-linked covalent organic framework. *J. Am. Chem. Soc.* **2013**, *135*, 17310–17313.
[51] Jackson, K. T.; Reich, T. E.; El-Kaderi, H. M. Targeted synthesis of a porous borazine-linked covalent organic framework. *Chem. Commun.* **2012**, *48*, 8823–8825.
[52] Bunck, D. N.; Dichtel, W. R. Bulk synthesis of exfoliated two-dimensional polymers using hydrazone-linked covalent organic frameworks. *J. Am. Chem. Soc.* **2013**, *135*, 14952–14955.
[53] Huang, N.; Chen, X.; Krishna, R.; Jiang, D. L. Two-dimensional covalent organic frameworks for carbon dioxide capture through channel-wall functionalization. *Angew. Chem., Int. Ed.* **2015**, *54*, 2986–2990.
[54] Pachfule, P.; Kandambeth, S.; Díaz, D. D.; Banerjee, R. Highly stable covalent organic framework-Au nanoparticles hybrids for enhanced activity for nitrophenol reduction. *Chem. Commun.* **2014**, *50*, 3169–3172.
[55] Furukawa, H.; Yaghi, O. M. Storage of hydrogen, methane, and carbon dioxide in highly porous covalent organic frameworks for clean energy applications. *J. Am. Chem. Soc.* **2009**, *131*, 8875–8883.
[56] Wei, P. F.; Qi, M. Z.; Wang, Z. P.; Ding, S. Y.; Yu, W.; Liu, Q.; Wang, L. K.; Wang, H. Z.; An, W. K.; Wang, W. Benzoxazole-linked ultrastable covalent organic frameworks for photocatalysis. *J. Am. Chem. Soc.* **2018**, *140*, 4623–4631.
[57] Pan, J.; Xu, Y. Y.; Yang, H.; Dong, Z. H.; Liu, H. F.; Xia, B. Y. Advanced architectures and relatives of air electrodes in Zn-air batteries. *Adv. Sci.* **2018**, *5*, 1700691.
[58] Arafat, Y.; Azhar, M. R.; Zhong, Y. J.; Abid, H. R.; Tadé, M. O.; Shao, Z. P. Advances in zeolite imidazolate frameworks (ZIFs) derived bifunctional oxygen electrocatalysts and their application in zinc-air batteries. *Adv. Energy Mater.* **2021**, *11*, 2100514.
[59] Jo, Y. N.; Kim, H. S.; Prasanna, K.; Ilango, P. R.; Lee, W. J.; Eom, S. W.; Lee, C. W. Effect of additives on electrochemical and corrosion behavior of gel type electrodes for Zn-air system. *Ind. Eng. Chem. Res.* **2014**, *53*, 17370–17375.
[60] Shao, M. H.; Chang, Q. W.; Dodelet, J. P.; Chenitz, R. Recent advances in electrocatalysts for oxygen reduction reaction. *Chem. Rev.* **2016**, *116*, 3594–3657.
[61] Davari, E.; Ivey, D. G. Bifunctional electrocatalysts for Zn-air batteries. *Sustainable Energy Fuels* **2018**, *2*, 39–67.
[62] Shu, X. X.; Chen, Q. W.; Yang, M. M.; Liu, M. M.; Ma, J. Z.; Zhang, J. T. Tuning Co-catalytic sites in hierarchical porous N-doped carbon for high-performance rechargeable and flexible Zn-air battery. *Adv. Energy Mater.* **2023**, *13*, 2202871.
[63] Guo, F. J.; Zhang, M. Y.; Yi, S. C.; Li, X. X.; Xin, R.; Yang, M.; Liu, B.; Chen, H. B.; Li, H. M.; Liu, Y. J. Metal-coordinated porous polydopamine nanospheres derived Fe_3N-FeCo encapsulated N-doped carbon as a highly efficient electrocatalyst for oxygen reduction reaction. *Nano Res. Energy* **2022**, *1*, e9120027.
[64] Dou, S.; Li, X. Y.; Tao, L.; Huo, J.; Wang, S. Y. Cobalt nanoparticle-embedded carbon nanotube/porous carbon hybrid derived from MOF-encapsulated Co_3O_4 for oxygen electrocatalysis. *Chem. Commun.* **2016**, *52*, 9727–9730.
[65] Gu, C. N.; Li, J. J.; Liu, J. P.; Wang, H.; Peng, Y.; Liu, C. S. Conferring supramolecular guanosine gel nanofiber with ZIF-67 for high-performance oxygen reduction catalysis in rechargeable zinc-air batteries. *Appl. Catal. B: Environ.* **2021**, *286*, 119888.
[66] Qian, Y. H.; Hu, Z. G.; Ge, X. M.; Yang, S. L.; Peng, Y. W.; Kang, Z. X.; Liu, Z. L.; Lee, J. Y.; Zhao, D. A metal-free ORR/OER bifunctional electrocatalyst derived from metal-organic frameworks for rechargeable Zn-air batteries. *Carbon* **2017**, *111*, 641–650.
[67] Liang, Z. Z.; Guo, H. B.; Zhou, G. J.; Guo, K.; Wang, B.; Lei, H. T.; Zhang, W.; Zheng, H. Q.; Apfel, U. P.; Cao, R. Metal-organic-framework-supported molecular electrocatalysis for the oxygen reduction reaction. *Angew. Chem., Int. Ed.* **2021**, *60*, 8472–8476.
[68] Zhang, W. D.; Hu, Q. T.; Wang, L. L.; Gao, J.; Zhu, H. Y.; Yan, X. D.; Gu, Z. G. *In-situ* generated Ni-MOF/LDH heterostructures with abundant phase interfaces for enhanced oxygen evolution reaction. *Appl. Catal. B: Environ.* **2021**, *286*, 119906.
[69] Salunkhe, R. R.; Kaneti, Y. V.; Kim, J.; Kim, J. H.; Yamauchi, Y. Nanoarchitectures for metal-organic framework-derived nanoporous carbons toward supercapacitor applications. *Acc. Chem. Res.* **2016**, *49*, 2796–2806.

[70] Chen, W. F.; Sasaki, K.; Ma, C.; Frenkel, A. I.; Marinkovic, N.; Muckerman, J. T.; Zhu, Y. M.; Adzic, R. R. Hydrogen-evolution catalysts based on non-noble metal nickel-molybdenum nitride nanosheets. *Angew. Chem., Int. Ed.* **2012**, *51*, 6131–6135.

[71] Amiinu, I. S.; Pu, Z. H.; Liu, X. B.; Owusu, K. A.; Monestel, H. G. R.; Boakye, F. O.; Zhang, H. N.; Mu, S. C. Multifunctional Mo-N/C@MoS_2 electrocatalysts for HER, OER, ORR, and Zn-air batteries. *Adv. Funct. Mater.* **2017**, *27*, 1702300.

[72] Yan, L. T.; Xu, Y. L.; Chen, P.; Zhang, S.; Jiang, H. M.; Yang, L. Z.; Wang, Y.; Zhang, L.; Shen, J. X.; Zhao, X. B. et al. A freestanding 3D heterostructure film stitched by MOF-derived carbon nanotube microsphere superstructure and reduced graphene oxide sheets: A superior multifunctional electrode for overall water splitting and Zn-air batteries. *Adv. Mater.* **2020**, *32*, 2003313.

[73] Li, J. J.; Xia, W.; Tang, J.; Gao, Y.; Jiang, C.; Jia, Y. N.; Chen, T.; Hou, Z. F.; Qi, R. J.; Jiang, D. et al. Metal-organic framework-derived graphene mesh: A robust scaffold for highly exposed Fe-N_4 active sites toward an excellent oxygen reduction catalyst in acid media. *J. Am. Chem. Soc.* **2022**, *144*, 9280–9291.

[74] Han, X. P.; Ling, X. F.; Wang, Y.; Ma, T. Y.; Zhong, C.; Hu, W. B.; Deng, Y. D. Generation of nanoparticle, atomic-cluster, and single-atom cobalt catalysts from zeolitic imidazole frameworks by spatial isolation and their use in zinc-air batteries. *Angew. Chem., Int. Ed.* **2019**, *58*, 5359–5364.

[75] Xu, Q.; Qian, J.; Luo, D.; Liu, G. J.; Guo, Y.; Zeng, G. F. Ni/Fe clusters and nanoparticles confined by covalent organic framework derived carbon as highly active catalysts toward oxygen reduction reaction and oxygen evolution reaction. *Adv. Sustain. Syst.* **2020**, *4*, 2000115.

[76] Liu, W. P.; Wang, C. M.; Zhang, L. J.; Pan, H. H.; Liu, W. B.; Chen, J.; Yang, D. J.; Xiang, Y. J.; Wang, K.; Jiang, J. Z. et al. Exfoliation of amorphous phthalocyanine conjugated polymers into ultrathin nanosheets for highly efficient oxygen reduction. *J. Mater. Chem. A* **2019**, *7*, 3112–3119.

[77] Park, J. H.; Lee, C. H.; Ju, J. M.; Lee, J. H.; Seol, J.; Lee, S. U.; Kim, J. H. Bifunctional covalent organic framework-derived electrocatalysts with modulated p-band centers for rechargeable Zn-air batteries. *Adv. Funct. Mater.* **2021**, *31*, 2101727.

[78] Li, W.; Wang, J. Y.; Chen, J. X.; Chen, K.; Wen, Z. H.; Huang, A. S. Core-shell carbon-based bifunctional electrocatalysts derived from COF@MOF hybrid for advanced rechargeable Zn-air batteries. *Small* **2022**, *18*, 2202018.

[79] Peng, P.; Shi, L.; Huo, F.; Mi, C. X.; Wu, X. H.; Zhang, S. J.; Xiang, Z. H. A pyrolysis-free path toward superiorly catalytic nitrogen-coordinated single atom. *Sci. Adv.* **2019**, *5*, eaaw2322.

[80] Zhao, X. J.; Pachfule, P.; Li, S.; Langenhahn, T.; Ye, M. Y.; Tian, G. Y.; Schmidt, J.; Thomas, A. Silica-templated covalent organic framework-derived Fe-N-doped mesoporous carbon as oxygen reduction electrocatalyst. *Chem. Mater.* **2019**, *31*, 3274–3280.

[81] Peng, P.; Shi, L.; Huo, F.; Zhang, S. J.; Mi, C. X.; Cheng, Y. H.; Xiang, Z. H. *In situ* charge exfoliated soluble covalent organic framework directly used for Zn-air flow battery. *ACS Nano* **2019**, *13*, 878–884.

[82] Xie, J. F.; Wang, Y. B. Recent development of CO_2 electrochemistry from Li-CO_2 batteries to Zn-CO_2 batteries. *Acc. Chem. Res.* **2019**, *52*, 1721–1729.

[83] Teng, X.; Niu, Y. L.; Gong, S. Q.; Xu, M. Z.; Liu, X.; Ji, L. L.; Chen, Z. F. In/ZnO@C hollow nanocubes for efficient electrochemical reduction of CO_2 to formate and rechargeable Zn-CO_2 batteries. *Mater. Chem. Front.* **2021**, *5*, 6618–6627.

[84] Xie, J. F.; Wang, X. Y.; Lv, J. Q.; Huang, Y. Y.; Wu, M. X.; Wang, Y. B.; Yao, J. N. Reversible aqueous zinc-CO_2 batteries based on CO_2-HCOOH interconversion. *Angew. Chem., Int. Ed.* **2018**, *57*, 16996–17001.

[85] Peng, M. Y.; Ci, S. Q.; Shao, P.; Cai, P. W.; Wen, Z. H. Cu_3P/C nanocomposites for efficient electrocatalytic CO_2 reduction and Zn-CO_2 battery. *J. Nanosci. Nanotechnol.* **2019**, *19*, 3232–3236.

[86] Teng, X.; Lu, J. M.; Niu, Y. L.; Gong, S. Q.; Xu, M. Z.; Meyer, T. J.; Chen, Z. F. Selective CO_2 reduction to formate on a Zn-based electrocatalyst promoted by tellurium. *Chem. Mater.* **2022**, *34*, 6036–6047.

[87] Peng, J. X.; Yang, W. J.; Jia, Z. H.; Jiao, L.; Jiang, H. L. Axial coordination regulation of MOF-based single-atom Ni catalysts by halogen atoms for enhanced CO_2 electroreduction. *Nano Res.* **2022**, *15*, 10063–10069.

[88] Jiao, L.; Zhu, J. T.; Zhang, Y.; Yang, W. J.; Zhou, S. Y.; Li, A. W.; Xie, C. F.; Zheng, X. S.; Zhou, W.; Yu, S. H. et al. Non-bonding interaction of neighboring Fe and Ni single-atom pairs on MOF-derived N-doped carbon for enhanced CO_2 electroreduction. *J. Am. Chem. Soc.* **2021**, *143*, 19417–19424.

[89] Abraham, K. M.; Jiang, Z. A polymer electrolyte-based rechargeable lithium/oxygen battery. *J. Electrochem. Soc.* **1996**, *143*, 1–5.

[90] Peng, Z. Q.; Freunberger, S. A.; Chen, Y. H.; Bruce, P. G. A reversible and higher-rate Li-O_2 battery. *Science* **2012**, *337*, 563–566.

[91] Lu, Y. C.; Gallant, B. M.; Kwabi, D. G.; Harding, J. R.; Mitchell, R. R.; Whittingham, M. S.; Shao-Horn, Y. Lithium-oxygen batteries: Bridging mechanistic understanding and battery performance. *Energy Environ. Sci.* **2013**, *6*, 750–768.

[92] Zhang, S. S.; Foster, D.; Read, J. Discharge characteristic of a non-aqueous electrolyte Li/O_2 battery. *J. Power Sources* **2010**, *195*, 1235–1240.

[93] Zhang, X. H.; Dong, P. P.; Lee, J. I.; Gray, J. T.; Cha, Y. H.; Ha, S.; Song, M. K. Enhanced cycling performance of rechargeable Li-O_2 batteries via LiOH formation and decomposition using high-performance MOF-74@CNTs hybrid catalysts. *Energy Storage Mater.* **2019**, *17*, 167–177.

[94] Liang, Z. B.; Qu, C.; Guo, W. H.; Zou, R. Q.; Xu, Q. Pristine metal-organic frameworks and their composites for energy storage and conversion. *Adv. Mater.* **2018**, *30*, 1702891.

[95] Li, Q.; Xu, P.; Gao, W.; Ma, S.; Zhang, G.; Cao, R.; Cho, J.; Wang, H. L.; Wu, G. Graphene/graphene-tube nanocomposites templated from cage-containing metal-organic frameworks for oxygen reduction in Li-O_2 batteries. *Adv. Mater.* **2014**, *26*, 1378–1386.

[96] Wu, D. F.; Guo, Z. Y.; Yin, X. B.; Pang, Q. Q.; Tu, B. B.; Zhang, L. J.; Wang, Y. G.; Li, Q. W. Metal-organic frameworks as cathode materials for Li-O_2 batteries. *Adv. Mater.* **2014**, *26*, 3258–3262.

[97] Lyu, Z. Y.; Lim, G. J. H.; Guo, R.; Kou, Z. K.; Wang, T. T.; Guan, C.; Ding, J.; Chen, W.; Wang, J. 3D-printed MOF-derived hierarchically porous frameworks for practical high-energy density Li-O_2 batteries. *Adv. Funct. Mater.* **2019**, *29*, 1806658.

[98] Jiang, Z. L.; Sun, H.; Shi, W. K.; Zhou, T. H.; Hu, J. Y.; Cheng, J. Y.; Hu, P. F.; Sun, S. G. Co_3O_4 nanocage derived from metal-organic frameworks: An excellent cathode catalyst for rechargeable Li-O_2 battery. *Nano Res.* **2019**, *12*, 1555–1562.

[99] Yuan, M. W.; Wang, R.; Fu, W. B.; Lin, L.; Sun, Z. M.; Long, X. G.; Zhang, S. T.; Nan, C. Y.; Sun, G. B.; Li, H. F. et al. Ultrathin two-dimensional metal-organic framework nanosheets with the inherent open active sites as electrocatalysts in aprotic Li-O_2 batteries. *ACS Appl. Mater. Interfaces* **2019**, *11*, 11403–11413.

[100] Meng, H. B.; Han, Y.; Zhou, C. H.; Jiang, Q. Y.; Shi, X. F.; Zhan, C. H.; Zhang, R. F. Conductive metal-organic frameworks: Design, synthesis, and applications. *Small Methods* **2020**, *4*, 2000396.

[101] Majidi, L.; Ahmadiparidari, A.; Shan, N.; Singh, S. K.; Zhang, C. J.; Huang, Z. H.; Rastegar, S.; Kumar, K.; Hemmat, Z.; Ngo, A. T. et al. Nanostructured conductive metal organic frameworks for sustainable low charge overpotentials in Li-air batteries. *Small* **2022**, *18*, 2102902.

[102] Choi, W. H.; Moon, B. C.; Park, D. G.; Choi, J. W.; Kim, K. H.; Shin, J. S.; Kim, M. G.; Choi, K. M.; Kang, J. K. Autogenous production and stabilization of highly loaded sub-nanometric particles within multishell hollow metal-organic frameworks and their utilization for high performance in Li-O_2 batteries. *Adv. Sci.* **2020**, *7*, 2000283.

[103] Hu, X. L.; Luo, G.; Zhao, Q. N.; Wu, D.; Yang, T. X.; Wen, J.; Wang, R. H.; Xu, C. H.; Hu, N. Ru single atoms on N-doped carbon by spatial confinement and ionic substitution strategies for high-performance Li-O_2 batteries. *J. Am. Chem. Soc.* **2020**, *142*, 16776–16786.

[104] Wang, X. X.; Chi, X. W.; Li, M. L.; Guan, D. H.; Miao, C. L.; Xu, J. J. Metal-organic frameworks derived electrolytes build multiple wetting interfaces for integrated solid-state lithium-oxygen battery. *Adv*. *Funct*. *Mater*. **2022**, *32*, 2113235.
[105] Qiao, Y.; He, Y. B.; Wu, S. C.; Jiang, K. Z.; Li, X.; Guo, S. H.; He, P.; Zhou, H. S. MOF-based separator in an Li-O_2 battery: An effective strategy to restrain the shuttling of dual redox mediators. *ACS Energy Lett*. **2018**, *3*, 463–468.
[106] Deng, H.; Chang, Z.; Qiu, F. L.; Qiao, Y.; Yang, H. J.; He, P.; Zhou, H. S. A safe organic oxygen battery built with Li-based liquid anode and MOFs separator. *Adv*. *Energy Mater*. **2020**, *10*, 1903953.
[107] Liu, Y. L.; Wang, R.; Lyu, Y. C.; Li, H.; Chen, L. Q. Rechargeable Li/CO_2-O_2 (2:1) battery and Li/CO_2 battery. *Energy Environ*. *Sci*. **2014**, *7*, 677–681.
[108] Mu, X. W.; Pan, H.; He, P.; Zhou, H. S. Li-CO_2 and Na-CO_2 batteries: Toward greener and sustainable electrical energy storage. *Adv*. *Mater*. **2020**, *32*, 1903790.
[109] Takechi, K.; Shiga, T.; Asaoka, T. A Li-O_2/CO_2 battery. *Chem*. *Commun*. **2011**, *47*, 3463–3465.
[110] Xu, S. M.; Das, S. K.; Archer, L. A. The Li-CO_2 battery: A novel method for CO_2 capture and utilization. *RSC Adv*. **2013**, *3*, 6656–6660.
[111] Hou, Y. Y.; Wang, J. Z.; Liu, L. L.; Liu, Y. Q.; Chou, S. L.; Shi, D. Q.; Liu, H. K.; Wu, Y. P.; Zhang, W. M.; Chen, J. Mo_2C/CNT: An efficient catalyst for rechargeable Li-CO_2 batteries. *Adv*. *Funct*. *Mater*. **2017**, *27*, 1700564.
[112] Zhou, J. W.; Li, X. L.; Yang, C.; Li, Y. C.; Guo, K. K.; Cheng, J. L.; Yuan, D. W.; Song, C. H.; Lu, J.; Wang, B. A quasi-solid-state flexible fiber-shaped Li-CO_2 battery with low overpotential and high energy efficiency. *Adv*. *Mater*. **2019**, *31*, 1804439.
[113] Xue, H. R.; Gong, H.; Lu, X. Y.; Gao, B.; Wang, T.; He, J. P.; Yamauchi, Y.; Sasaki, T.; Ma, R. Z. Aqueous formate-based Li-CO_2 battery with low charge overpotential and high working voltage. *Adv*. *Energy Mater*. **2021**, *11*, 2101630.
[114] Li, S. W.; Dong, Y.; Zhou, J. W.; Liu, Y.; Wang, J. M.; Gao, X.; Han, Y. Z.; Qi, P. F.; Wang, B. Carbon dioxide in the cage: Manganese metal-organic frameworks for high performance CO_2 electrodes in Li-CO_2 batteries. *Energy Environ*. *Sci*. **2018**, *11*, 1318–1325.
[115] Dong, L. Z.; Zhang, Y.; Lu, Y. F.; Zhang, L.; Huang, X.; Wang, J. H.; Liu, J.; Li, S. L.; Lan, Y. Q. A well-defined dual Mn-site based metal-organic framework to promote CO_2 reduction/evolution in Li-CO_2 batteries. *Chem*. *Commun*. **2021**, *57*, 8937–8940.
[116] Xu, Y. Y.; Gong, H.; Ren, H.; Fan, X. L.; Li, P.; Zhang, T. F.; Chang, K.; Wang, T.; He, J. P. Highly efficient Cu-porphyrin-based metal-organic framework nanosheet as cathode for high-rate Li-CO_2 battery. *Small* **2022**, *18*, 2203917.
[117] Lei, Z. D.; Xue, Y. C.; Chen, W. Q.; Qiu, W. H.; Zhang, Y.; Horike, S.; Tang, L. MOFs-based heterogeneous catalysts: New opportunities for energy-related CO_2 conversion. *Adv*. *Energy Mater*. **2018**, *8*, 1801587.
[118] Huang, S.; Chen, D. D.; Meng, C.; Wang, S. J.; Ren, S.; Han, D. M.; Xiao, M.; Sun, L. Y.; Meng, Y. Z. CO_2 nanoenrichment and nanoconfinement in cage of imine covalent organic frameworks for high-performance CO_2 cathodes in Li-CO_2 battery. *Small* **2019**, *15*, 1904830.
[119] Li, X.; Wang, H.; Chen, Z. X.; Xu, H. S.; Yu, W.; Liu, C. B.; Wang, X. W.; Zhang, K.; Xie, K. Y.; Loh, K. P. Covalent-organic-framework-based Li-CO_2 batteries. *Adv*. *Mater*. **2019**, *31*, 1905879.
[120] Jana, A.; Bähring, S.; Ishida, M.; Goeb, S.; Canevet, D.; Sallé, M.; Jeppesen, J. O.; Sessler, J. L. Functionalised tetrathiafulvalene-(TTF-) macrocycles: Recent trends in applied supramolecular chemistry. *Chem*. *Soc*. *Rev*. **2018**, *47*, 5614–5645.
[121] Zhang, Y.; Zhong, R. L.; Lu, M.; Wang, J. H.; Jiang, C.; Gao, G. K.; Dong, L. Z.; Chen, Y. F.; Li, S. L.; Lan, Y. Q. Single metal site and versatile transfer channel merged into covalent organic frameworks facilitate high-performance Li-CO_2 batteries. *ACS Cent*. *Sci*. **2021**, *7*, 175–182.
[122] Cheng, F. Y.; Chen, J. Metal-air batteries: From oxygen reduction electrochemistry to cathode catalysts. *Chem*. *Soc*. *Rev*. **2012**, *41*, 2172–2192.
[123] Peled, E.; Golodnitsky, D.; Hadar, R.; Mazor, H.; Goor, M.; Burstein, L. Challenges and obstacles in the development of sodium-air batteries. *J*. *Power Sources* **2013**, *244*, 771–776.
[124] Zu, C. X.; Li, H. Thermodynamic analysis on energy densities of batteries. *Energy Environ*. *Sci*. **2011**, *4*, 2614–2624.
[125] Peled, E.; Golodnitsky, D.; Mazor, H.; Goor, M.; Avshalomov, S. Parameter analysis of a practical lithium-and sodium-air electric vehicle battery. *J*. *Power Sources* **2011**, *196*, 6835–6840.
[126] Sun, Q.; Yang, Y.; Fu, Z. W. Electrochemical properties of room temperature sodium-air batteries with non-aqueous electrolyte. *Electrochem*. *Commun*. **2012**, *16*, 22–25.
[127] Hartmann, P.; Bender, C. L.; Sann, J.; Dürr, A. K.; Jansen, M.; Janek, J.; Adelhelm, P. A comprehensive study on the cell chemistry of the sodium superoxide (NaO_2) battery. *Phys*. *Chem*. *Chem*. *Phys*. **2013**, *15*, 11661–11672.
[128] Hartmann, P.; Bender, C. L.; Vračar, M.; Dürr, A. K.; Garsuch, A.; Janek, J.; Adelhelm, P. A rechargeable room-temperature sodium superoxide (NaO_2) battery. *Nat*. *Mater*. **2013**, *12*, 228–232.
[129] Das, S. K.; Xu, S. M.; Archer, L. A. Carbon dioxide assist for non-aqueous sodium-oxygen batteries. *Electrochem*. *Commun*. **2013**, *27*, 59–62.
[130] Xu, S. M.; Lu, Y. Y.; Wang, H. S.; Abruña, H. D.; Archer, L. A. A rechargeable Na-CO_2/O_2 battery enabled by stable nanoparticle hybrid electrolytes. *J*. *Mater*. *Chem*. *A* **2014**, *2*, 17723–17729.
[131] Wu, Y. Q.; Qiu, X. C.; Liang, F.; Zhang, Q. K.; Koo, A.; Dai, Y. N.; Lei, Y.; Sun, X. L. A metal-organic framework-derived bifunctional catalyst for hybrid sodium-air batteries. *Appl*. *Catal*. *B*: *Environ*. **2019**, *241*, 407–414.
[132] Hu, M.; Reboul, J.; Furukawa, S.; Torad, N. L.; Ji, Q. M.; Srinivasu, P.; Ariga, K.; Kitagawa, S.; Yamauchi, Y. Direct carbonization of Al-based porous coordination polymer for synthesis of nanoporous carbon. *J*. *Am*. *Chem*. *Soc*. **2012**, *134*, 2864–2867.
[133] Xia, B. Y.; Yan, Y.; Li, N.; Wu, H. B.; Lou, X. W.; Wang, X. A metal-organic framework-derived bifunctional oxygen electrocatalyst. *Nat*. *Energy* **2016**, *1*, 15006.
[134] Zhu, J. Y.; Qu, T.; Su, F. M.; Wu, Y. Q.; Kang, Y.; Chen, K. F.; Yao, Y. C.; Ma, W. H.; Yang, B.; Dai, Y. N. et al. Highly dispersed Co nanoparticles decorated on a N-doped defective carbon nano-framework for a hybrid Na-air battery. *Dalton Trans*. **2020**, *49*, 1811–1821.
[135] Yeo, B. S.; Bell, A. T. Enhanced activity of gold-supported cobalt oxide for the electrochemical evolution of oxygen. *J*. *Am*. *Chem*. *Soc*. **2011**, *133*, 5587–5593.
[136] Zaromb, S.; Foust, R. A. Jr. Feasibility of electrolyte regeneration in Al batteries. *J*. *Electrochem*. *Soc*. **1962**, *109*, 1191.
[137] Zaromb, S. The use and behavior of aluminum anodes in alkaline primary batteries. *J*. *Electrochem*. *Soc*. **1962**, *109*, 1125.
[138] Mokhtar, M.; Talib, M. Z. M.; Majlan, E. H.; Tasirin, S. M.; Ramli, W. M. F. W.; Daud, W. R. W.; Sahari, J. Recent developments in materials for aluminum-air batteries: A review. *J*. *Ind*. *Eng*. *Chem*. **2015**, *32*, 1–20.
[139] Li, J. S.; Zhou, N.; Song, J. Y.; Fu, L.; Yan, J.; Tang, Y. G.; Wang, H. Y. Cu-MOF-derived Cu/Cu_2O nanoparticles and CuN_xC_y species to boost oxygen reduction activity of ketjenblack carbon in Al-air battery. *ACS Sustain*. *Chem*. *Eng*. **2018**, *6*, 413–421.
[140] Liu, Y. S.; Jiang, H.; Hao, J. Y.; Liu, Y. L.; Shen, H. B.; Li, W. Z.; Li, J. Metal-organic framework-derived reduced graphene oxide-supported ZnO/$ZnCo_2O_4$/C hollow nanocages as cathode catalysts for aluminum-O_2 batteries. *ACS Appl*. *Mater*. *Interfaces* **2017**, *9*, 31841–31852.
[141] Ma, J. L.; Bao, D.; Shi, M. M.; Yan, J. M.; Zhang, X. B. Reversible nitrogen fixation based on a rechargeable lithium-nitrogen battery for energy storage. *Chem* **2017**, *2*, 525–532.
[142] Barthram, A. M.; Cleary, R. L.; Kowallick, R.; Ward, M. D. A new redox-tunable near-IR dye based on a trinuclear ruthenium(II) complex of hexahydroxytriphenylene. *Chem*. *Commun*. **1998**, *24*, 2695–2696.

[143] Hmadeh, M.; Lu, Z.; Liu, Z.; Gándara, F.; Furukawa, H.; Wan, S.; Augustyn, V.; Chang, R.; Liao, L.; Zhou, F. et al. New porous crystals of extended metal-catecholates. *Chem. Mater.* **2012**, *24*, 3511–3513.
[144] Gu, S. N.; Bai, Z. W.; Majumder, S.; Huang, B. L.; Chen, G. H. Conductive metal-organic framework with redox metal center as cathode for high rate performance lithium ion battery. *J. Power Sources* **2019**, *429*, 22–29.
[145] Bai, Y.; Liu, C. L.; Shan, Y. Y.; Chen, T. T.; Zhao, Y.; Yu, C.; Pang, H. Metal-organic frameworks nanocomposites with different dimensionalities for energy conversion and storage. *Adv. Energy Mater.* **2022**, *12*, 2100346.
[146] Zhu, D. Y.; Xu, G. Y.; Barnes, M.; Li, Y. L.; Tseng, C. P.; Zhang, Z. Q.; Zhang, J. J.; Zhu, Y. F.; Khalil, S.; Rahman, M. M. et al. Covalent organic frameworks for batteries. *Adv. Funct. Mater.* **2021**, *31*, 2100505.

Yunyun Xu received her bachelor's degree in Materials Chemistry from Fuyang Normal University in 2020, and continually studied for Master in Physical Chemistry at Nanjing University of Aeronautics and Astronautics. Her current research direction includes Li-CO_2 batteries and the application of photocatalysis.

Hairong Xue received his B.S. (2009), M.S. (2012) and PhD (2016) degrees at the College of Material Science and Technology, Nanjing University of Aeronautics and Astronautics (NUAA, China). He worked as a lecturer at College of Chemical Engineering, Zhejiang University of Technology (ZJUT, China) after graduation. Since 2018, he has worked in the group of Prof. Renzhi Ma at National Institute for Materials Science (NIMS, Japan) as a Postdoctoral Fellow. His research interest centers on developing functional materials for energy storage and convention.

Tao Wang received his PhD degree in Materials Physics and Chemistry from Nanjing University of Aeronautics and Astronautics (NUAA) in 2012. From 2013-2015, he worked in Prof. Jinhua Ye's group as a postdoctoral fellow at the National Institute for Materials Science, Japan. After that he took associate professor position in NUAA. His current research interest focuses on the design, preparation, and application of the porous materials for photoelectrochemical catalysis.

Jianping He received his PhD from Nanjing University of Aeronautics and Astronautics (NUAA) in 2001, and joined NUAA in 1988. He is now a Professor at NUAA and the President of Nanjing Surface Treatment Research Association, Vice president of Nanjing Surface treatment Industry Association. He is mainly engaged in the research of new energy materials and electrochemistry, functional film preparation and stealth materials, environmental performance evaluation of materials.